existing fiber optic networks without much insertion loss. Moreover, the range of operation of the filter can be shifted with entire C- and L- band by changing the initial parameters of the grating at the time of fabrication. Furthermore, the surface relief grating does not decay with time like index gratings and thus, the properties of filter do not change over time. Additionally, $LiNbO_3$ is insensitive to the IR wavelengths and thus even continuous illumination of the filter does not alter its properties. Another important parameter of the filter is selectivity which is ranging between 150 pm to 200 pm. By changing the grating length and with some apodization, this value can be controlled. The interchannel spacing used in present DMDM networks is 800 pm and thus the presented filter even with shorter grating length (implies increased bandwidth sufficient to fit within 800 pm range) can be used for dropping a single channel in DMDM networks. However, to avoid crosstalk between the neighboring channels, the sidelobes should be completely suppressed and this can be done by increased apodization of the grating, i.e. by further decreasing the grating amplitude on edges as compared to the central section of the grating. Another important parameter is the ripple of the transfer function. The signal to noise ratio (SNR) of the amplitude of the transmitted or reflected signal affects the quality of the signal and the data throughput of a channel. The realized filter transfer functions as shown in Figs. 5.27 and 5.29 exhibit no visible ripples i.e., small distortions of the amplitude of the signal. Furthermore, the measured transfer functions exhibit spectral stability, i.e., the spectral position of the transfer function is stable within a pew picometer. However, the parameters discussed above are important concerning the telecommunication applications which are very stringent. Considering the fact that the realized filter fulfills most of the requirements for telecommunications, it is very attractive for applications like wavelength locking and stabilization of lasers and also for high resolution spectroscopic measurements.

5.4 Nonlinear Photorefractive Gratings

This section is an extension of section 5.3.1 where an integrated optical filter based on volume photorefractive grating was discussed. It is known that volume photorefractive gratings, when read out in reflection geometry exhibit highly selective spectral response with a narrow bandwidth. This fact was checked and established in section 5.3.1 where a filter based on photorefractive grating in lithium niobate channel waveguide with almost 100% diffraction efficiency and narrow bandwidth (0.16 nm) was realized. Such integrated optical filters based on photorefractive reflection gratings are promising for DWDM applications, the influence of spatial nonlinearities on the spectral response of such filters is still questionable, though. In this section, the detailed investigation on detection of diffraction from higher nonlinear harmonics of photorefractive waveguide gratings [116, 117] is discussed.

It is well known that the photorefractive recording is a nonlinear process leading to nonsinusoidal refractive index response to the incident sinusoidal interference intensity pattern.

This implies the existence of higher spatial harmonics in photorefractive gratings. Especially, in the case of high modulation depth, the resulting refractive index response is highly nonlinear [118]. As discussed in section 5.3.1, the diffraction efficiency was quite high (almost 100%) and the modulation depth was close to 1. This fact triggered the idea of investigation of nonlinear harmonics of the realized photorefractive gratings. Diffraction from the nonlinear components of photorefractive gratings in transmission geometry has been investigated many times [119–122]. The high angular selectivity of the transmission geometry makes it possible to exploit the angular dependence of diffraction for the investigation of nonlinearities. As most of the applications of photorefractive gratings are based on reflection, it becomes critical to investigate the influence of nonlinearities also in reflection geometry. Unlike transmission, the reflection geometry is not very sensitive to angular variations. This fact makes it difficult to detect and investigate nonlinearities in the reflection geometry.

I used a comprehensive and clever technique for detecting diffraction from the higher nonlinear spatial harmonic components of photorefractive gratings in reflection geometry. Here we exploited the inherited high wavelength selectivity of the reflection geometry to investigate the wavelength dependence of diffraction from the fundamental and higher harmonics. The theoretical formulation, experimental technique used and the results are discussed in detail in next sections.

5.4.1 Theoretical Formulation

We consider a volume grating with periodical variations of the refractive index defined as

$$n = n_{\text{av}} + n_1 \cos Kx; K = 2(\pi/\Lambda), \tag{5.25}$$

where n_{av} is the average refractive index of the material, n_1 is the amplitude of the periodic modulation of the refractive index and K is the grating wavevector. The diffraction from such a grating obeys the well-known Bragg condition [3, 13, 15]. For the case of normal incidence (direction of propagation is parallel to the grating vector) of light on such a grating (reflection geometry), the Bragg condition is mathematically stated as [3]:

$$\lambda_{\text{B}} = 2n_{\text{av}}\Lambda \tag{5.26}$$

where n_{av} is the average refractive index of the material at λ_{B}, Λ is the grating period as shown in Fig. 5.30(a). For the case of nonlinear gratings (Fig. 5.30(b)) having higher spatial nonlinear components, the Bragg condition has a more general form:

$$m\lambda_{\text{B}} = 2n_{\text{av}}\Lambda \tag{5.27}$$

where m is an integer. The appearance of the factor m results due to the existence of the higher spatial harmonics $2K, 3K, ...$and so on. In spite of the simplicity of eqn. (5.27), it is not easy to detect the wavelength dependence of diffraction from higher harmonics.

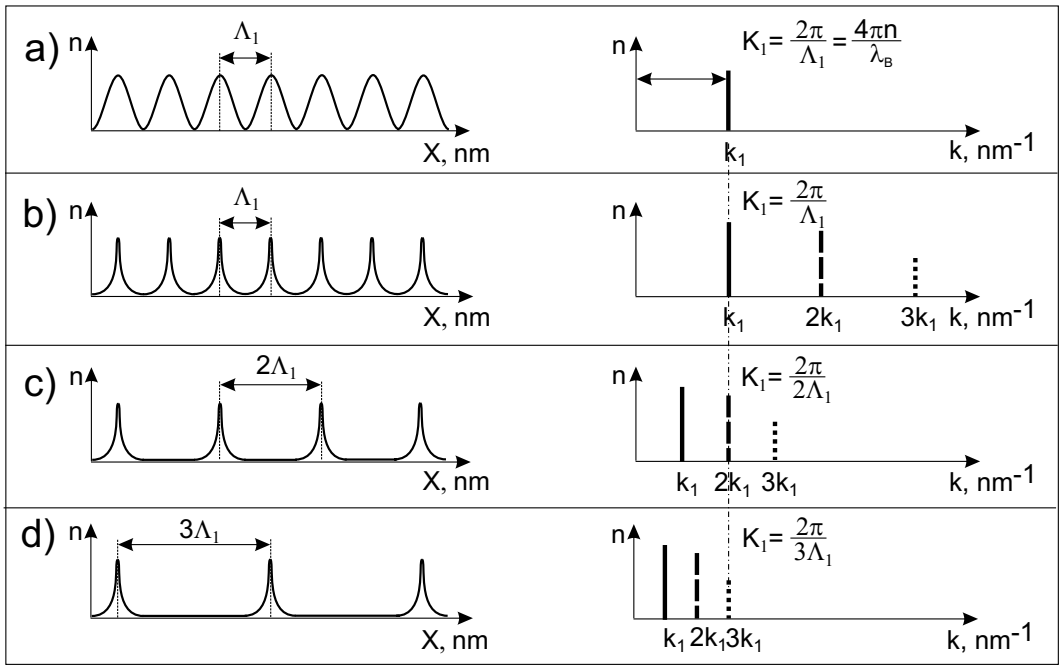

Figure 5.30: Grating profile (left) and its spectrum (right). (a) Sinusoidal grating with the grating period Λ_1 containing a single Fourier component. To observe diffraction from this grating in the reflection geometry, the read-out wavelength λ_B must be fitted to the grating wavevector K_1. (b) Strongly nonlinear grating with the same grating period Λ_1, containing higher spatial Fourier components. (c) Strongly nonlinear grating with the grating period $2\Lambda_1$. The second nonlinear component $2K_1$ is fitted to the read-out wavelength λ_B. (d) Strongly nonlinear grating with the grating period $3\Lambda_1$. The third nonlinear component $3K_1$ is fitted to the read-out wavelength λ_B.

For example, one can see that in order to investigate the diffraction from higher nonlinear harmonic components (Fig. 5.30(b)), one has to have different light sources with suited wavelengths as the wavelength diffracted will be different for different harmonics. To have different light sources with a wavelength matching exactly wavelength diffracted from different harmonics, is practically impossible.

In order to detect diffraction from higher nonlinear harmonics, an innovative technique was used: at first, a grating with the period Λ_I fitting to the readout Bragg wavelength λ_B is recorded. At the second step, the recording angle was changed to record another grating with the grating period $\Lambda_{II} = 2 \cdot \Lambda_I$. The fundamental grating period now is Λ_{II} and this grating period does not fit with the readout Bragg wavelength λ_B. However, we assume the existence of the higher nonlinear harmonic components of the grating (for example, via the photorefractive effect). This implies the appearance of the second order nonlinear grating component with the grating period $\Lambda_{II}/2$. In the ideal case, this component should

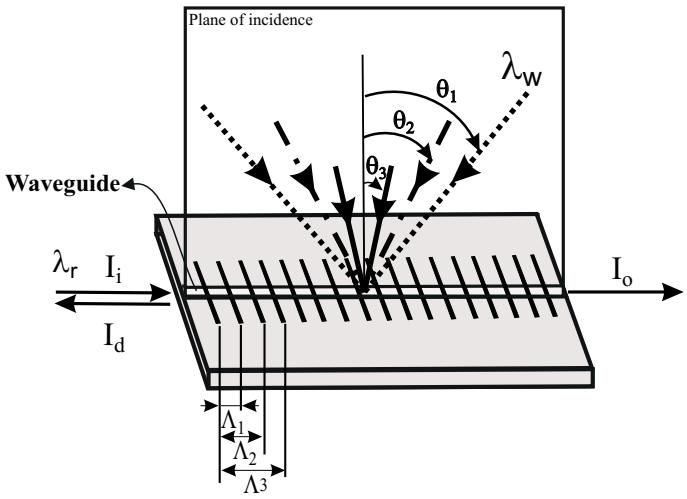

Figure 5.31: Experimental geometry for the write and the read-out process. λ_w, λ_r are the write and read-out wavelengths; I_i, I_o, I_d are the input, output and diffracted beams, respectively. θ_1, θ_2 and θ_3 are the half angles between the interfering beams, writing the gratings with grating periods Λ_1, Λ_2 and Λ_3, respectively.

be exactly fitted to the readout Bragg wavelength λ_B as shown in Fig. 5.30(c), i.e.

$$\lambda_B = 2n_{av}\Lambda_I = 2n_{av}\left(\frac{\Lambda_{II}}{2}\right) \tag{5.28}$$

At the third step, the recording angle was changed again in order to record another grating with a period $\Lambda_{III} = 3 \cdot \Lambda_I$. Following the same consideration, the appearance of the third order nonlinear component is expected, which is fitted again to the readout Bragg wavelength λ_B as shown in Fig. 5.30(d), i.e.

$$\lambda_B = 2n_{av}\Lambda_I = 2n_{av}\left(\frac{\Lambda_{II}}{2}\right) = 2n_{av}\left(\frac{\Lambda_{III}}{3}\right) \tag{5.29}$$

In general case, we can write:

$$\lambda_B = 2n_{av}\left(\frac{\Lambda_m}{m}\right) \tag{5.30}$$

where the grating period Λ_m is defined via the writing wavelength λ_w and the angle θ between the recording beams

$$\Lambda_m = m \cdot \frac{\lambda_w}{2\sin\theta} \tag{5.31}$$

It is important to note that in each step as described above, all nonlinear components are existing simultaneously in time. However, with the suggested technique, each component was separately detected from different gratings, by step by step fitting of each nonlinear component to the fixed readout Bragg wavelength. Using this technique, we used just one light source (laser) and detected diffraction from three higher harmonics.

5.4.2 Experimental Set-up

The experimental technique consisted of two parts. In the first step, a photorefractive grating was recorded into the waveguide using the transmission geometry as discussed in section 5.3.1. A Ti-indiffused single mode channel waveguide in a lithium niobate crystal ($10mm \times 8mm \times 1mm$) with single-mode fibers connected at each end of the waveguide (as shown in Fig. 5.14) was used (to ensure perfect reflection geometry for the read-out).

In the second step, the recorded grating was read-out in reflection geometry to investigate the transmission spectrum. For the recording of the photorefractive gratings, two expanded coherent plane beams (each with 6 mm diameter) of an argon-ion laser at a wavelength of $\lambda = 458$ nm were used. The two beams were then directed by two mirrors such that they interfere in the waveguide to record the photorefractive index grating in transmission geometry. Initially an interbeam angle of $2\theta_1 = 81.359^\circ \pm 0.005^\circ$ was chosen using the technique of the precise angular calibration [123].

Using eqn. (5.31), the recorded grating has a period of $\Lambda_1 = 351.320 \pm 0.02$ nm for the used angle θ_1. The read-out process was done in reflection geometry using a tunable infrared laser. Strong diffraction from the fundamental harmonic was observed at the Bragg wavelength $\lambda_{\mathrm{B}}(exp.) = 1554.47$ nm. Using eqn. (5.26) and the experimentally observed value of the Bragg wavelength for the first harmonic, we calculated the average refractive index of the material (waveguide in our case) $n_{\mathrm{av}} = 2.212 \pm 0.0001$. After the measurements, the grating was erased.

To observe diffraction from the second harmonic, another Photorefractive grating with two times the grating period of the earlier grating (corresponding to the fundamental harmonic) was recorded. The interbeam angle was changed to $2\theta_2 = 38.367^\circ \pm 0.005^\circ$ to change the grating period as shown in Fig. 5.31. This grating had a grating period of $\Lambda_2 = 696.907 \pm 0.09$ nm. The grating period for the second harmonic component was then $(\Lambda_2/2) = 348.454 \pm 0.04$ nm. This grating period for the second harmonic was chosen to be little different from the grating period for the fundamental harmonic in order to avoid any influence of the previous experiment. The read-out was then done again in reflection geometry and efficient diffraction was observed from this second harmonic component at $\lambda_{\mathrm{B}}(exp.) = 1546.17$ nm. In addition to the experimentally observed Bragg wavelength, the theoretical Bragg wavelength was estimated to be $\lambda_{\mathrm{B}}(theo.) = 1541.81$ nm, using the calculated average refractive index (as discussed above) and eqn. (5.26). The obvious difference between the experimental and the theoretically predicted Bragg wavelength indicated "Bragg wavelength shift" for the second harmonic.

To observe diffraction from the third harmonic, another photorefractive grating with three times the grating period of the first grating (corresponding to the fundamental harmonic) was recorded. The inter-beam angle was changed to $2\theta_3 = 25.002^\circ \pm 0.005^\circ$ to change the grating period as shown in figure 2. This grating had a grating period of $\Lambda_3 = 1057.949 \pm 0.21$ nm. The grating period for the third harmonic component was then $(\Lambda_3/3) = 352.650 \pm 0.07$ nm.

The grating period for the third harmonic was again chosen to be little different from the grating period for the fundamental and the second harmonic in order to avoid any influence of the previous experiments. The read-out was then done again in reflection geometry and a diffracted signal was observed from this third harmonic component at $\lambda_{\mathrm{B}}(exp.) = 1580.55$ nm. Here again, the theoretical Bragg wavelength was estimated to be $\lambda_{\mathrm{B}}(theo.) = 1560.37$ nm, using the calculated average refractive index and eqn. (5.26). Bragg wavelength shift was observed for the third harmonic as well. Using the proposed technique, the diffraction was observed in the same wavelength range, from the first, second and the third harmonic of three different gratings with different fundamental grating periods, respectively.

5.4.3 Detection of Higher Harmonics

As discussed in the previous section, strong diffraction from the fundamental harmonic of the grating was observed and more than 90% diffraction efficiency was easily observed in all attempts. $10 - 12\%$ diffraction efficiency was observed for the second harmonic diffraction and approximately $4 - 6\%$ diffraction efficiency was observed for third harmonic diffraction. It was not possible to detect diffraction from other higher order harmonic components as the diffraction efficiency of a higher harmonic index grating decreases by one order of magnitude per harmonic order. Vachss et al. [118] have discussed the nonlinear photorefractive response in great detail. Using the experimental data and the theoretical model presented in [118], the space-charge fields for the first, second and third harmonic was estimated and was approximately 52.2 kV/cm, 6.9 kV/cm and 4.3 kV/cm, respectively. The decrease in the strength of the space-charge field for the higher harmonics leads to the reduced amplitude and hence, the reduced diffraction efficiency of the higher harmonics.

Fig. 5.32 shows the spectral response of the diffracted signal for the first three harmonics. In each case, the experimentally measured results were compared to the theoretical simulations done using the Kogelnik's theory [13]. Kogelnik's theory [13, 15] was used for comparing the diffraction from each harmonic separately, as we considered higher harmonics as individual gratings with different grating amplitudes. The parameters used for the fitting are mentioned with each plot in Fig. 5.32. It can be seen that the grating amplitude n_1 decreases for each higher harmonic and this implies weaker gratings with lower diffraction efficiencies. The length of the grating T is different for all three fittings and it is due to the fact that the angle between the beams writing the grating was different each time (as explained in the former section). For the first harmonic, there is a good fit between theory and experiment except the absence of side lobes in the experimental plot. This can be attributed to an apodized grating i.e. the amplitude of the grating is not constant over the whole length of the grating. Kogelnik's theory considers only non-apodized gratings and hence side lobes are prominently seen. However, the absence of side lobes can also be due to absorption. But, absorption was very weak for the used sample and therefore was neglected.

For the second harmonic, there is again a good fit between theory and experiment, but side lobes are not clearly distinguishable here as well. For the third harmonic, the fitting is not appropriate. The central peak of the spectral response is much broader than that predicted by theory. This can be attributed to the instabilities during the recording process. The recording time was longest (about 3 hours) for observing a diffracted signal from the third harmonic and therefore, presence of instabilities can be significant, leading to a broadening of the central peak in the spectral response. Moreover, as the diffraction efficiency was quiet low for higher harmonics as compared to the fundamental harmonic, the signal to noise ratio decreased leading to a poor matching of the experimental results to the theoretical results for the second and the third harmonic.

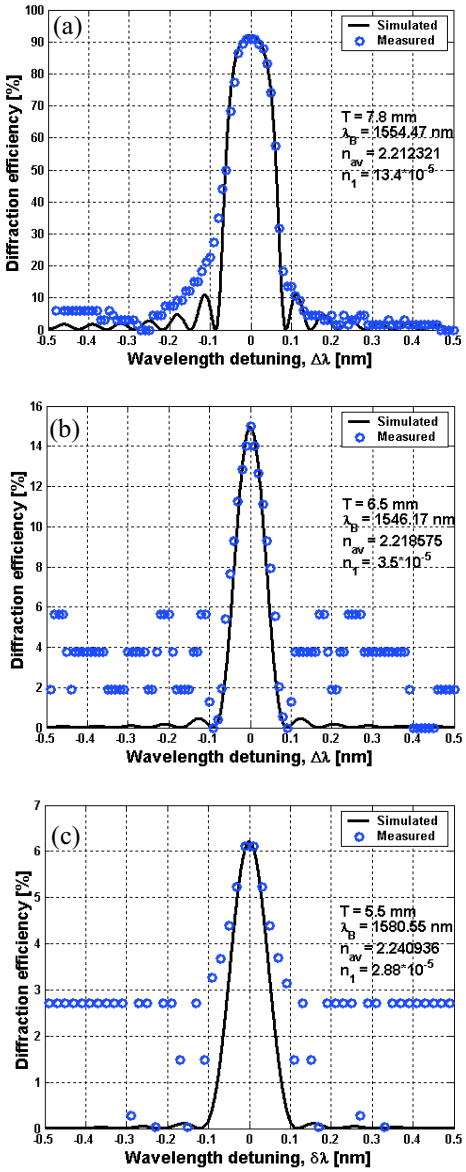

Figure 5.32: Spectral response of the signal diffracted in reflection for the (a) first harmonic, (b) second harmonic, (c) third harmonic.

The dependence of the experimentally measured Bragg wavelength shift on the order of nonlinearity is presented in Fig. 5.33. This phenomenon of "Bragg wavelength shift" can be explained as the influence of the homogeneous photovoltaic effect on the Bragg condition for volume holograms in $LiNbO_3$ [124, 125]. An additional component of the electric field, E_{pvh} appears during the photorefractive recording process, due to the photovoltaic effect. The value of this additional field depends on parameters of the grating being recorded. Thus the value of the photovoltaic field will be different for the three gratings recorded with different parameters and so the change in the refractive index of the material will be different for the three gratings and the affect on the Bragg condition will also be different. The maximum value of photovoltaic field for lithium niobate

reported in literature is 100 KV/cm [124]. Although, the photovoltaic effect is stronger in waveguides [126] but exact values of the field are not mentioned. Some other effects alongwith the photovoltaic effect can also be responsible for the wavelength shift. However, this shift in the Bragg wavelength is crucial and should be taken into account for the applications based on the nonlinear photorefractive effect.

Figure 5.33: Dependence of the Bragg wavelength shift on the order of nonlinearity.

The results reported in this section are important for all applications based on Photorefractive gratings. The photorefractive nonlinearity is undesirable for some applications as some of the light will be diffracted to higher harmonics as well. However, it can be useful for some applications where a grating with period smaller than that can be realized even with perfect reflection geometry of recording. It is known that a minimum grating period can be obtained by use of a pair of counterpropagating beams, leading to a grating period of $\Lambda = \lambda/2n_{av}$, where n_{av} is the average refractive index of the recording medium. Due to the efficient diffraction from the higher-harmonic components of the photorefractive gratings, as reported in this section, it is possible to use gratings with grating periods smaller than $\lambda/2n_{av}$. However, methods can be developed to increase the photorefractive nonlinearity and hence the amplitude and the diffraction efficiency of the higher-harmonics.

Chapter 6

Phase Shift Keying

In this chapter, the concept of phase-shift keying will be introduced, which is used to increase the functionality of grating-based filters as discussed in the previous chapter. The coupled-wave theory of phase-shifted gratings is briefly presented. Furthermore, the implementation of the concept using electrical control of the fabricated grating-filter will be discussed in detail. Such a technique provides very fast dynamic control and synthesis of the transfer function with a reconfiguration time typically less than 1μs. In addition, some of the potential applications of the phase-shifted Bragg gratings will be discussed.

6.1 Introduction

With the continuous progress of optical communication systems, there is an ever increasing demand for higher speeds and more bandwidth. Optical multiplexing techniques like wavelength-division multiplexing (WDM) and time-division multiplexing (TDM) have been adopted in order to cater to higher speed and bandwidth requirements. But these conventional techniques require dedication of one wavelength per user and strict temporal synchronization of the networks, respectively [127]. With the exhaust of the available frequencies in the transmission window of the transporting optical fibers, new and more appropriate multiplexing techniques are being explored for further bandwidth enhancement. Recently developed optical code-division multiple access (OCDMA) is one such technique which permits many channels to share the same wavelength band but to be individually addressable through the allocation of specific address codes [128]. With the evolution of such dynamically reconfigurable networks, there is a need for reconfigurable optical devices such as multiplexers, encoders, decoders, cross-connects, tunable filters with dynamic control and enhanced functionality. The discussion here, however, will be restricted to devices based on Bragg gratings. As discussed in chapter 5, Bragg gratings due to their high selectivity and narrow bandwidth are commonly used as optical wavelength/frequency filters.

A dynamic control of the reflection wavelength and the shape of the spectral transfer function of the grating filter is desirable for a variety of applications in telecommunications. One of the recently reported demonstration of a reconfigurable encoder-decoder based on a uniform fiber Bragg grating [127] is a promising development for OCDMA networks. The continuous phase-shifting property of the reported device is being explored for the use in multilevel phase-shift keying operation of the network. Due to the increasing demand, various techniques for inducing temporary or permanent phase-shifts to gratings are being explored. Here, I propose one such technique based on electro-optic effect, for inscribing phase-shifts in corrugated waveguide gratings in lithium niobate. As the name suggests, phase-shift keying refers to grating with phase shifted cells. With the electro-optical phase shift keying [129,130] of the integrated Bragg grating, as will be discussed in next sections, it is possible to dynamically synthesize or reconfigure the spectral transfer function of the grating based filter.

6.2 Theoretical Concept of Phase-Shift Keying

As discussed in chapter 4 and 5, the reflected spectrum or the spectral response of a Bragg grating has the shape of a very narrow peak and thus the grating acts as a stop-band or notch optical filter. However, if there are phase, grating-spacing or average refractive index discontinuities, the shape of the spectral transfer function can be transformed and acquires a complicated form, for instance, some transmission maxima may arise inside the stop-band. In general, the spectral transfer function can be controlled by a change of the period, the refractive index or the amplitude of the whole grating or by spatial modulation of the period, the phase or the amplitude of the grating.

A technique with which the different section of a grating are shifted in phase with respect to each other is what we call as phase-shift keying of a grating. With this technique, the spectral transfer function of the grating is synthesized or reconfigured by the spatial phase modulation of the grating. A grating with phase shifted sections can be represented as several small homogeneous gratings with different phases. The total amplitude of the reflected or transmitted light will be the coherent sum of amplitudes of light reflected or transmitted by each homogeneous grating cell. The reflected or transmitted signal then strongly depends on the number of the phase shifted sections and the magnitude of phase-shift between different homogeneous grating sections. Fig. 6.1 illustrates the basic principle of the phase-shift keying concept. For a simple homogeneous grating (as shown in Fig. 6.1(a)), the light with wavelength λ_B will be completely reflected (as shown in Fig. 6.1(b)). If the phase of half of the same homogeneous grating is shifted with respect to the other half as shown in Fig. 6.1(c), the light reflected from the grating planes in the two phase shifted sections will also be shifted in phase. For a phase difference of π between the two sections, the light reflected from the one section will be totally out of phase with light reflected from the other section and will result in destructive interference of light with

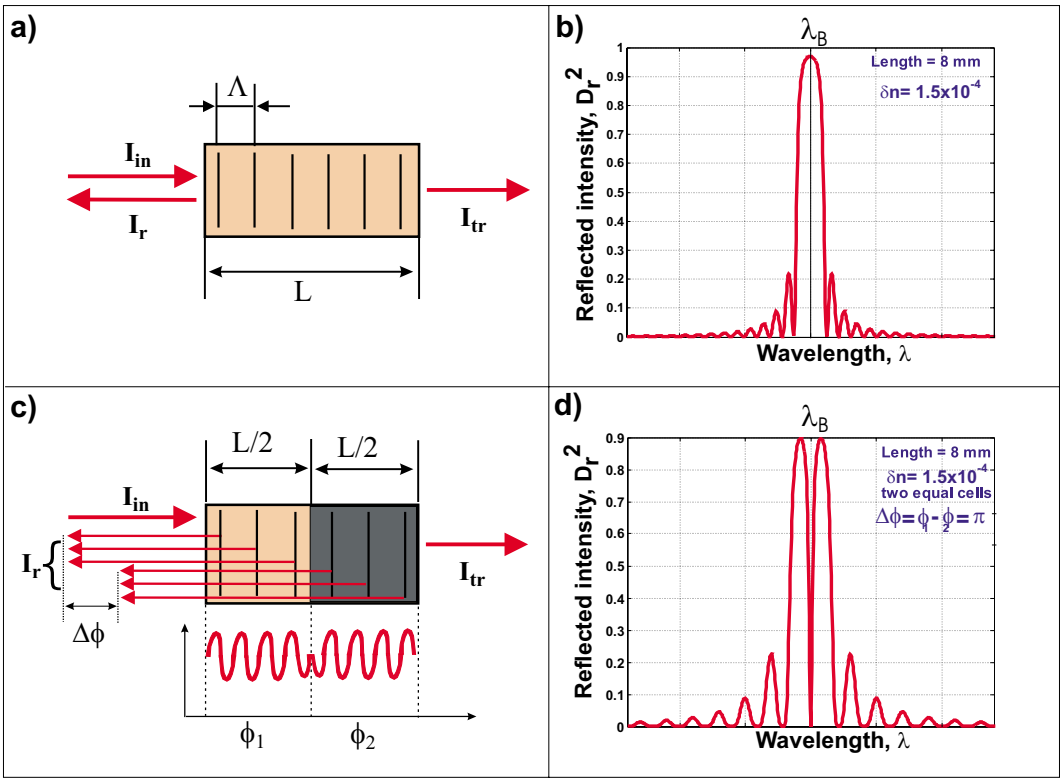

Figure 6.1: The basic principle of phase-shift keying. (a) A Bragg grating with period Λ and length L; I_{in}, I_r and I_{tr} are the input, reflected and the transmitted light intensities, respectively. (b) Dependence of the reflection coefficient (D_r^2) on wavelength for the grating shown in (a). (c) A refractive index grating with same parameters as for the grating shown in (a) and with two phase shifted sections: section of $L/2$ length with phase ϕ_1 and section of length $L/2$ with phase ϕ_2. (d) Dependence of the reflection coefficient (D_r^2) on wavelength for the grating with two halves shifted in phase by π with each other as shown in (c).

the wavelength λ_B and will lead to total transmission instead of total reflection of light at this wavelength as shown in Fig. 6.1(d). With a phase shift of π introduced between the two grating halves, the spectral transfer function, therefore, is switched from reflection to transmission mode. This reconfiguration of transfer function done using phase-shift keying of two grating halves can also be seen as switching from the stop-band to pass-band in reflection or vice-versa in transmission. The narrow transmission band that appears at the Bragg wavelength due to used phase-shift keying scheme has a bandwidth narrower than the bandwidth of the original transfer function. The example shown here demonstrates the basic principle of phase-shift keying and exhibits the potential of this technique in realizing narrow bandwidth transfer function. However depending on the number of sections and magnitude of phase shift, several other modes of transfer function with complex profiles can be synthesized as discussed in next section. The more the number of sections and the range of magnitude of phase-shift, the better would be the flexibility in demonstrating

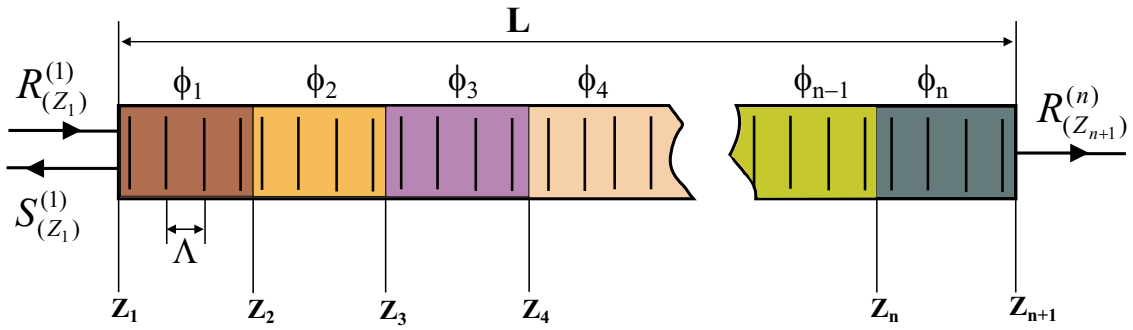

Figure 6.2: General geometry of a Bragg grating with n phase shifted cells. The Z_1,Z_2,....,Z_n,Z_{n+1} are the boundaries of the cells, ϕ_n is the phase shift of the nth cell, Λ is the grating period, L is the length of the grating, $R^{(1)}_{(Z_1)}$, $S^{(1)}_{(Z_1)}$, and $R^{(n)}_{(Z_{n+1})}$ are the complex amplitudes of the incident, reflected and transmitted wave, respectively.

variety of interesting transfer function reconfigurations.

6.2.1 Coupled Wave Theory of Phase Shifted Bragg Gratings

A uniform grating with phase shifted cells is also referred to as structured or segmented Bragg grating as it has the same period and amplitude over its entire length but contains phase jumps. The coupled-mode theory developed by Kogelnik [13] for uniform Bragg grating with no phase jumps was discussed in Section 2.3.1 in chapter 2. This theory now can be further extended to segmented Bragg gratings in order to predict their characteristic behavior. This extended coupled-mode theory was developed by C. Heinisch et al. [131] in 2005 and for detailed description and explanation on this theory, the reader is referred to [132–134]. The authors adopt this theory for phase shifted holographic Bragg gratings. However, the theory is generalized for all types of phase shifted grating types. It is important to briefly describe this theory before proceeding to the numerical simulations.

We consider a uniform Bragg reflection grating of length L and with n phase shifted cells as shown in Fig. 6.2. Z_n and Z_{n+1} represent the boundaries of nth cell and ϕ_i with i = 1,2,3....,n represent the specific phase of each cell. Such a grating can be represented as linear combination of n homogeneous gratings and so the coupled-mode equations (eqn. (2.21) and eqn. (2.22)) have to be solved for each of the n gratings individually. Following the same approach as discussed in Section 2.3.1 in chapter 2, the general solution for the nth cell is given as

$$R^{(n)}(Z) = R_1^{(n)} \exp(\gamma_1 Z) + R_2^{(n)} \exp(\gamma_2 Z) \tag{6.1}$$

$$S^{(n)}(Z) = S_1^{(n)} \exp(\gamma_1 Z) + S_2^{(n)} \exp(\gamma_2 Z) \tag{6.2}$$

where the constants $R_1^{(n)}$, $R_2^{(n)}$, $S_1^{(n)}$, and $S_2^{(n)}$ are the constants which are determined by the boundary conditions. There are n-1 boundary conditions between the neighboring

grating cells and are expressed as

$$R^{(n)}(Z_{n+1}) = R^{(n+1)}(Z_{n+1}) \qquad for \quad n = 1, 2, ..., n-1 \tag{6.3}$$

$$S^{(n)}(Z_{n+1}) = S^{(n+1)}(Z_{n+1}) \qquad for \quad n = 1, 2, ..., n-1 \tag{6.4}$$

Using the coupled equations (2.21) and (2.22) alongwith the phase factors $\phi(Z)$ and equations (6.1) and (6.2) results in

$$\begin{aligned} &R_1^{(n)} \exp(\gamma_1 Z_{n+1}) + R_2^{(n)} \exp(\gamma_2 Z_{n+1}) \\ &- R_1^{(n+1)} \exp(\gamma_1 Z_{n+1}) - R_2^{(n+1)} \exp(\gamma_2 Z_{n+1}) = 0 \end{aligned} \tag{6.5}$$

$$\begin{aligned} &R_1^{(n)} \exp(\gamma_1 Z_{n+1} + i\phi_n).\gamma_1 \\ &+ R_2^{(n)} \exp(\gamma_2 Z_{n+1} + i\phi_n).\gamma_2 \\ &- R_1^{(n+1)} \exp(\gamma_1 Z_{n+1} + i\phi_{n+1}).\gamma_1 \\ &- R_2^{(n+1)} \exp(\gamma_2 Z_{n+1} + i\phi_{n+1}).\gamma_2 = 0 \end{aligned} \tag{6.6}$$

There are two additional boundary conditions for the reflection geometry: $S^{(n)}(Z_{n+1}) = 0$ as there is no light diffracted from the outer boundary of the last cell and $R^{(1)}(Z_1) = 1$ as the incident wave is assumed to enter with amplitude 1. Inserting these boundary conditions in equation (2.21), (2.22), (6.1) and (6.2) yields

$$R_1^{(1)} \exp(\gamma_1 Z_1) + R_2^{(1)} \exp(\gamma_2 Z_1) = 1 \tag{6.7}$$

$$R_1^{(n)} \exp(\gamma_1 Z_{n+1}).\gamma_1 + R_2^{(n)} \exp(\gamma_2 Z_{n+1}).\gamma_2 = 0. \tag{6.8}$$

The complex amplitudes for the incident and the diffracted waves at the entry point can be calculated by inserting eqn. (6.1) for n = 1 into eqn. (2.21) which yields

$$R^{(1)}(Z_1) = R_1^{(1)} \exp(\gamma_1 Z_1) + R_2^{(1)} \exp(\gamma_2 Z_1) \tag{6.9}$$

$$S^{(1)}(Z_1) = (i/\kappa) \exp(i\phi_1)[R_1^{(1)} \exp(\gamma_1 Z_1).\gamma_1 + R_2^{(1)} \exp(\gamma_2 Z_1).\gamma_2]. \tag{6.10}$$

It is important to define the spectral transfer function of the grating, which is expressed as the ratio of the complex amplitude of the diffracted wave and the complex amplitude of the incident wave at the entry point

$$\xi(\lambda) = \frac{S^{(1)}(Z_1)}{R^{(1)}(Z_1)}. \tag{6.11}$$

However, the experimentally measured quantity is the diffraction efficiency as a function of the wavelength, which is defined as the square of the modulus of ξ

$$\eta(\lambda) = \mid \xi(\lambda) \mid^2 . \tag{6.12}$$

6.2.2 Numerical Simulations

After discussing the theory of phase shifted gratings, some numerical simulations were done in order to check the spectral transfer function of a grating with different numbers of phase shifted cells and with different magnitude of the phases. The theory as explained above was used to iteratively calculate the diffraction efficiency or the transfer function. Fig. 6.3 illustrates some of the transfer function reconfigurations numerically simulated for different phase combinations. These reconfigurations demonstrate the potential of the phase-shift keying technique for the dynamic control of the reflected wavelength and the shape of the transfer function. Such reconfigurations of the transfer function can be very useful e.g. for channel selection and separation in modern telecommunication networks, tunable lasers, dynamic interferometry, optical sensors etc.

6.3 Experimental Implementation

In the previous section, the potential of the phase-shift keying of Bragg gratings was demonstrated. In this section, the methods to implement this technique experimentally will be discussed.

An overview of existing techniques

In general, a phase-shift can be introduced by interrupting the periodicity of the refractive index or the period of the grating. The principle of the phase-shifted grating was first introduced in 1986 by Alferness et. al. in periodic structures made form semiconductor materials where a phase shift was introduced by etching a larger spacing at the center of a single uniform grating to produce two grating halves with an uncorrugated section between them of reduced waveguide thickness [135]. Such a structure provided a grating with two sections shifted in phase by $\pi/2$, resulting in the appearance of a very narrow transmission peak (a few GHz) inside a relatively broad reflection band. This result relaxed the requirement of long grating structures in order to have narrow bandwidth filters. Moreover, filter based on phase-shifted gratings work in transmission rather than reflection. The so-produced phase-shifted grating, also known as distributed feedback grating was next used for mode-control of semiconductor DFB laser [136]. J. Canning et. al. later used the technique of phase-shift keying for fiber Bragg gratings by raising the general refractive index at a certain region in the fiber Bragg grating through irradiation with UV light [137]. At the same time, R. Kashyap et. al. used the phase-shifted phase mask technique to inscribe a phase-shift into the fiber grating [138]. Thermal post-processing was also used to introduce phase shifts in fiber gratings as discussed by M. Janos et. al. [139]. The above mentioned techniques for phase-shift keying of fiber Bragg gratings inscribe permanent phase shifts. However, temporary phase shifts can be introduced into the fiber grating by

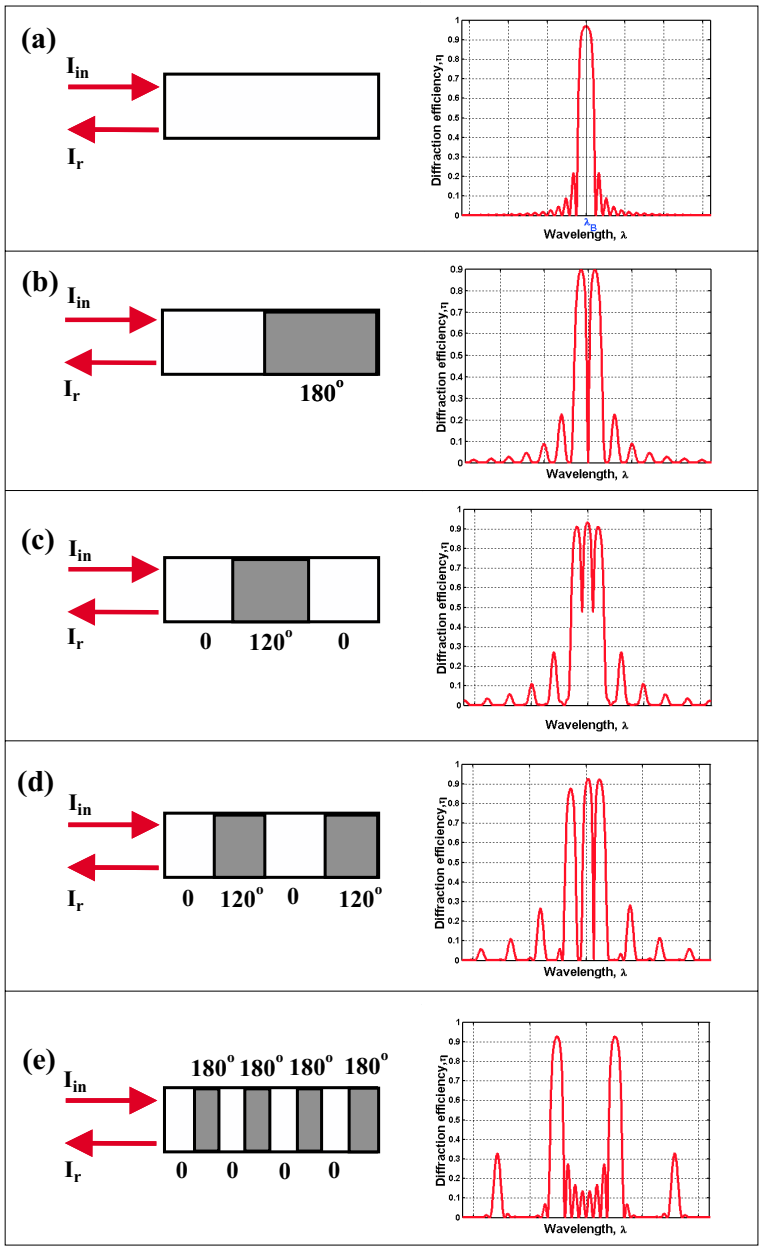

Figure 6.3: Spectral transfer function reconfigurations for different phase combinations simulated for an index grating of length 8 mm, with modulation strength $\delta n = 1.5\ X\ 10^{-4}$ and period 352 nm. Left column shows the phase distribution over the grating length and right column shows the corresponding transfer function.

external disturbances such as heating (via thermo-optic effect) [140, 141] or tension [142]. For an illustrious reference on fiber Bragg gratings and their spectral characteristics, the reader is referred to [143].

Recently polymer based waveguide gratings have drawn interest as they provide a low-cost solution for optical filters. In order to produce multi-channel bandpass filters in polymer waveguides, Wang et. al. used a phase-shifted phase mask to interferometrically record phase-shifted Bragg gratings in a polymer waveguide [144]. In 2004, Zhu et. al. proposed direct e-beam writing to make corrugated sidewall Bragg gratings in polymer waveguides and demonstrated phase-shifted passband filters by introducing defects in the grating structure [145].

The technique of phase-shift keying has also been used for volume holographic (photorefractive gratings) in bulk $BaTiO_3$ crystal by Petrov et. al., where a liquid crystal phase modulator was used in the path of the recording beam in order to record dynamic phase-shifted grating [146]. The similar technique was further extended by Heinisch et. al. where a phase modulator with large number of cells was used in order to reconfigure several modes of the transfer function [131]. A practical application of such phase-shifted holographic Bragg gratings for dynamic interferometry was proposed by Lichtenberg et. al. [147].

Electro-optical phase-shift keying

Most of the above mentioned techniques for the implementation of phase-shift keying either introduce permanent phase shifts already at the time of grating fabrication or temporary phase shifts to already fabricated gratings via external forces like heating or tension. The permanently induced phase-shift leave no possibility to dynamically reconfigure the transfer function later on and a grating with required phase-shift has to be specially fabricated in order to realize a desired reconfiguration. The real-time and temporary phase-shifts introduced by heating or tension do not give exactly predictable response and reconfiguration times are in the range of a few seconds. Use of a phase-modulator in dynamic holography as mentioned above provides an efficient solution with a large number of phase-shifted cells but is limited by the response (writing and erasing time) of the crystal used which is typically in the range of a few seconds. Moreover, this scheme was used for dynamic holographic set-up which is not very convenient for use in existing communication networks. However, considering the applications of phase-shifted gratings for modern telecommunication networks, switching time is a crucial parameter. Phase-shifted gratings based on fiber or integrated-optical design are definitely preferred due to efficient inclusion in the existing optical fiber based networks.

As discussed in section 4.7 in chapter 4, using electrical control, switching times in the range of few hundred microseconds can be achieved. In the case of integrated optical implementation with electrical control, the switching time can be pushed to nanoseconds range which is a desired for many applications. In chapter 5, the electrical control of waveguide gratings was already discussed for tuning of the spectral transfer function. I, here, extended the concept of electrical control to implement the phase-shift keying for the already fabricated waveguide gratings. The biggest advantage of the proposed technique

is that one single homogeneous grating is used to exhibit dynamic and fast control of the transfer function. In addition, there are no mechanical movements required for reconfiguring the transfer function making the technique additionally fast and effective. Moreover, it offers a great deal of flexibility and dynamical control at the operational level as the induced phase-shifts are controlled by externally applied voltage to the electrodes leading to a real-time complex transfer function reconfigurations.

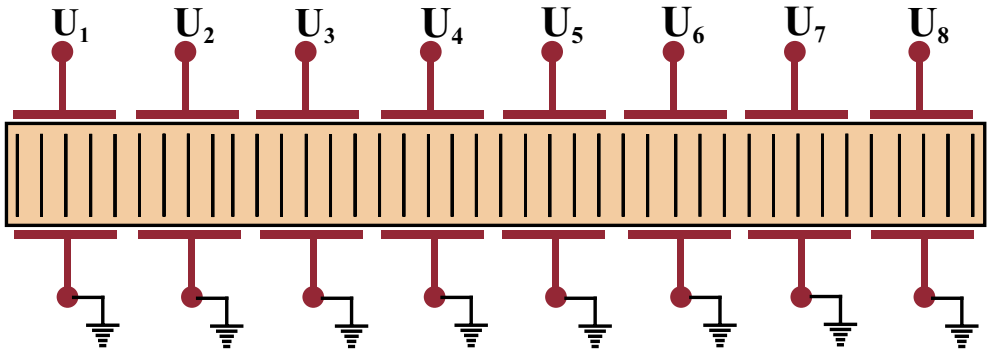

Figure 6.4: Phase-shift keying of a grating via electro-optic effect. U_1, U_2,...,U_8 represent the voltage applied to 8 electrode pairs, respectively.

The externally applied field leads to a local change in the average refractive index of $LiNbO_3$ via the electro-optic effect. Instead of applying a homogeneous electric field, a spatial distribution of the electric field leads to spatial distribution of the refractive index ultimately leading to a phase distribution over the structure, which is nothing but phase-shift keying. For tuning the transfer function, an electrode was deposited on either side of the waveguide as discussed in the previous chapter. In order to implement phase-shift keying, more than one electrodes of equal length were deposited on either side of the waveguide. The number of electrode pairs used will lead to an equal number of grating cells as shown in Fig. 6.4. By applying different combinations of electrical voltages to different electrodes, a different amount of phase-shift can be introduced to each grating section and by doing this, the spectral transfer function can be tailored (or reconfigured or synthesized). As this technique exploits the electro-optic effect, we call it electro-optical phase-shift keying. The advantages of this technique over other methods for phase-shift keying are the simple realization as only pairs of electrodes have to deposited along the already fabricated grating, the dynamic control as just by changing the applied voltages, the phase-shift and hence the spectral transfer function can be tailored. One of the biggest advantage is the fast operation as it is based on the electro-optic effect.

We implemented this technique for fixed or corrugated waveguide gratings as for photorefractive waveguide gratings, this technique was already used by Petrov et. al. [92], where 2 electrode pairs along the waveguide were used to control the transfer function. As the fabricated gratings had an effective length of 8 mm, 8 electrode pairs of 1 mm each with 50 μm spacing were deposited along the waveguide. After deposition, the single-mode fiber

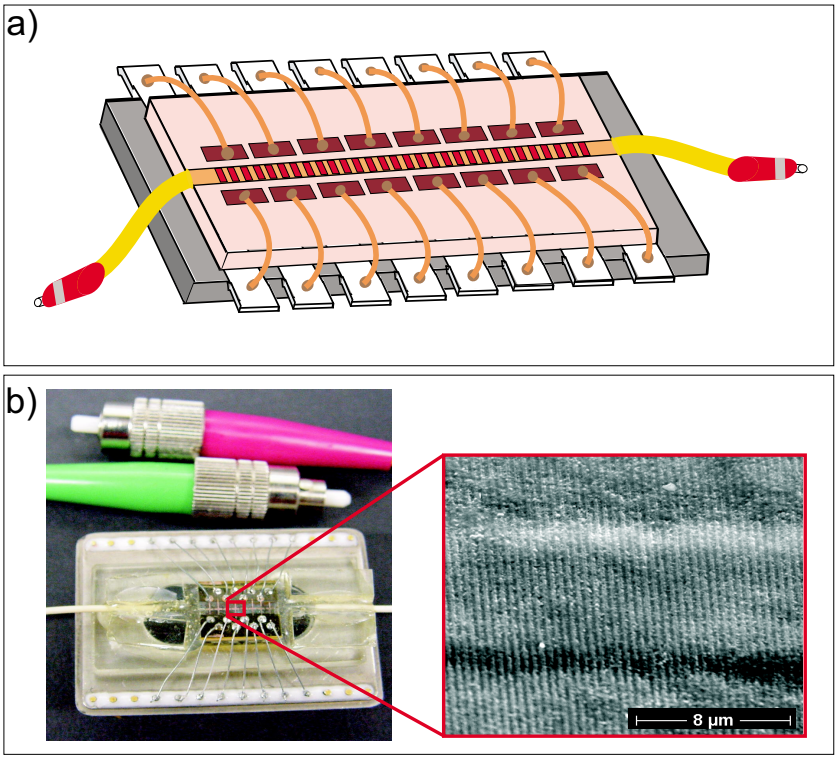

Figure 6.5: a) Layout of the filter based on a waveguide grating alongwith 8 electrode pairs for the electro-optical phase-shift keying of the waveguide grating and b) picture of the assembled filter with a corrugated waveguide grating shown in the scanning electron micrograph.

patch cables were attached to the ends of the waveguide and the crystal was packaged in a protective cover as shown in Fig. 6.5. A power supply box with eight independent voltage supplies was used in order to apply a voltage to each electrode separately. A Labview program was used to control the voltage on each electrode independently. The range of the applied voltage was limited to $\pm$ 10 V/μm in order to avoid the limit of breakdown voltage.

6.4 Transfer Function Reconfigurations

As discussed in the previous section, the electro-optical phase-shift keying provides dynamical control at the operational level. Various transfer function reconfigurations could be demonstrated by changing the electrical field from -10 V/μm to +10 V/μm on each of the 8 electrodes. Some of the realized reconfigurations e.g. continuous tuning of a single selected channel, reconfiguration from pass-band to stop-band, reconfiguration from one to two, three and five pass-bands, reconfiguration to a flat-top profile, dynamic correction

of the transfer function profile, dynamic control of the bandwidth and the shape of the transfer function are presented in this section.

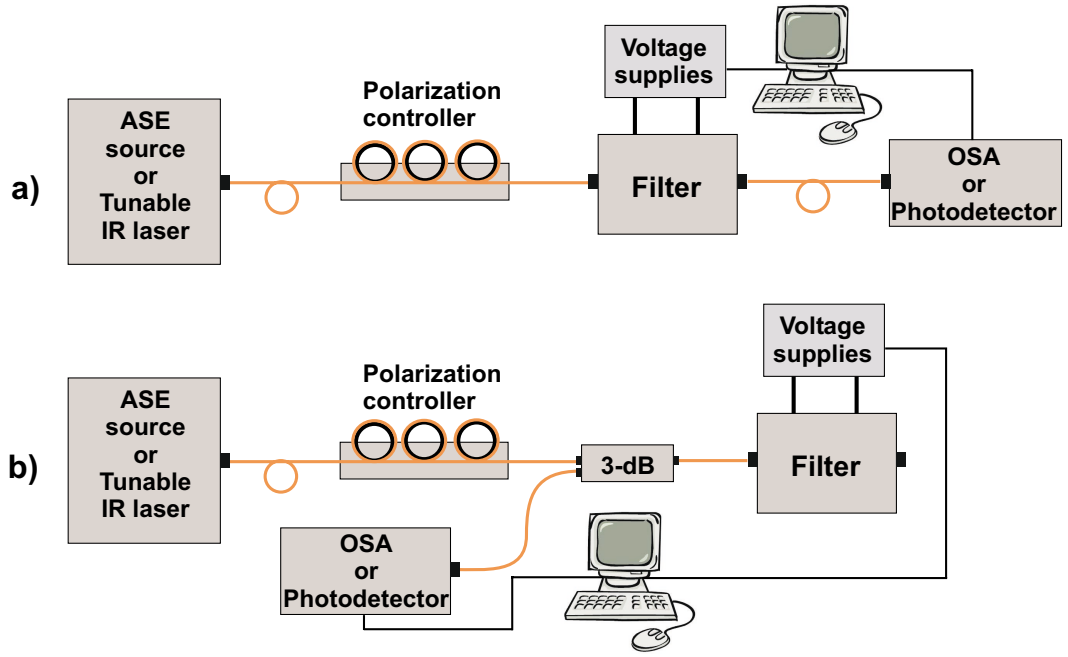

Figure 6.6: Measurement set-up: a) in transmission and b) in reflection.

The set-up used for the measurements in transmission and reflection are shown in Fig. 6.6. As discussed in section 5.3.2 in chapter 5, either a tunable IR laser or a ASE (Amplified Stimulated Emission) broadband source were used for the read-out and a photodetector or an OSA (Optical Spectrum Analyzer) were used as a detector to measure the reflection or the transmission spectrum. The transfer matrix method [148, 149] was utilized in order to analyze the transmission characteristics of the phase-shifted Bragg gratings. The measured results were theoretically verified for a surface grating with a length of 8 mm and a period of 352 nm. The theoretical simulation was done using the transfer matrix method for structured waveguide gratings. The grating was divided in 8 sections of 1 mm each and an appropriate electric field was used for each section according to the scheme of electro-optical phase-shift keying used for a particular reconfiguration. The effective electro-optic coefficient and the effect of apodization was also taken into consideration.

6.4.1 Tunable Single Wavelength Filter

A uniform Bragg grating is intrinsically a single wavelength filter. Fig. 6.7(a) shows the transfer function of the corrugated waveguide grating realized in a Ti:$LiNbO_3$ waveguide using the technological sequence discussed in section 5.3.2 in chapter 5. The solid line represents the simulated data and filled circles represent the measured data. The length of

the grating was 8 mm, the period was about 352 nm. The Bragg wavelength is 1555.15 nm and the FWHM (full width at half maximum) is 0.16 nm. The peak diffraction efficiency was more than 95%. The height of the first strong sidelobe is about 20% of the main peak. Such a filter can be potentially used for dropping a single channel from a broad spectrum and can also be used to filter a single mode from a laser. When an external electric field

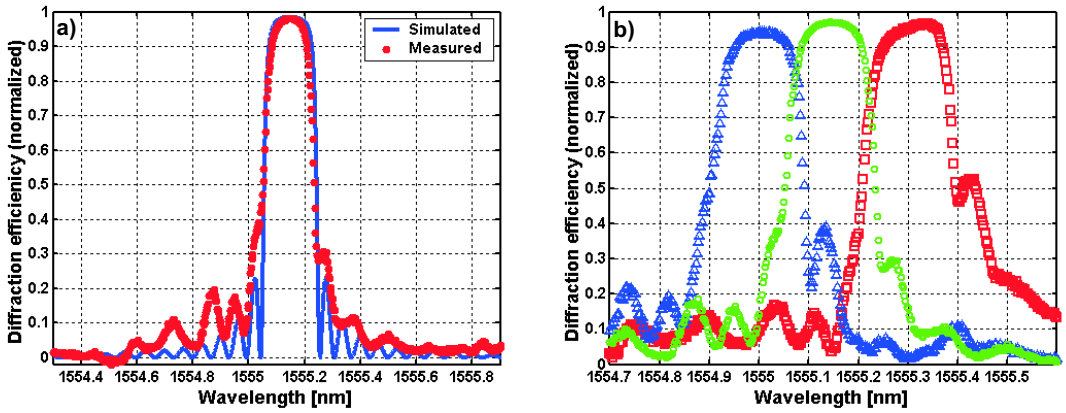

Figure 6.7: a) Measured transfer function of the grating filter as compared to the simulated function and b) electrical tuning of the filter transfer function- △: E = +10 V/μm; ○: E = 0; □: E = -10 V/μm.

is applied to the waveguide, the refractive index changes via the electro-optic effect and the central Bragg wavelength shifts. In this case, an equal voltage was applied to all the 8 electrodes in order to tune the central peak wavelength of the filter. Fig. 6.7(b) shows the tuning of the single wavelength filter. The triangles represent the measured data when an electric field of +10 V/μm was applied on all electrodes, the squares represent the data when an electric field of -10 V/μm was applied on all electrodes, and the circles represent the original transfer function when no external field was applied. The measured data is shown only for two values of the electric field. However, continuous tuning is possible for all intermediate values of the applied field. The experiments showed a continuous tuning of the central wavelength in the range of ±0.3 nm with a maximum applied field of ±10 V/μm. Such a tunable single channel filter could be used for various applications such as spectroscopy, tunable lasers, telecommunications etc.

6.4.2 Multi-Channel Filter

Tuning of a single channel was achieved by applying a homogeneous electric field all over the grating length as it was discussed in section 5.3 in chapter 5 or by applying the same voltage to all the electrodes as discussed in previous section. In this section, the potential of electro-optical phase-shift keying will be used to synthesize two-channel, three-channel and five-channel transfer functions. The splitting of a single diffraction peak into two

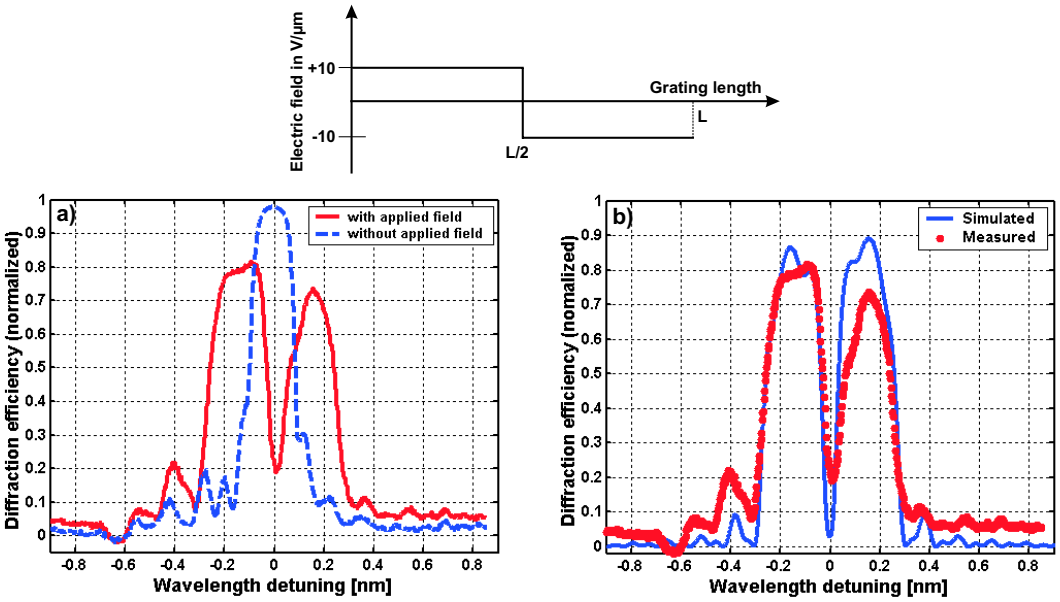

Figure 6.8: Synthesis of a two channel filter with the electro-optically applied phase-shift scheme as shown above the plots: a) Measured transfer function of the grating filter without (dashed) and with (solid) applied electric field and b) experimentally measured (filled circles) with theoretically simulated (solid) transfer function.

peaks, achieved by applying an equal and opposite value of the electric field on two halves of the grating, is shown in Fig. 6.8. The central minimum of the transfer function realized with applied electric field coincides with the maximum of the original transfer function as shown in Fig. 6.8(a). This is the stop-band to pass-band reconfiguration as was discussed in section 6.2. The applied phase-shift keying scheme is shown over the plots. The two peaks represent two channels that can be filtered with such a reconfiguration. The spectral separation between the peaks was 0.25 nm. A comparison with the theoretical result confirms the measured result as the position of the measured peaks coincides with the positions predicted by the theory. However, the value of the electric field used for the theoretical simulation was less than that was actually applied. This is due to the reason that the field lines do not effectively penetrate the entire waveguide as the waveguide is raised above the surface (by about 200 nm) due to titanium indiffusion. With a better electrode geometry, the same result can be produced with lower values of the applied field. One more thing to note is that the theory predicts two peaks of equal strength and bandwidth but the measured result differs with this prediction. This is attributed to the fact that the grating realized was not homogeneous all over its length and there are some phase errors in the fabrication process of such long gratings. Another important aspect of this filter manipulation is that the filter can be used as a switch as on the application of such electrically inscribed phase-shift, the filter switches from the reflection to the transmission mode at the same wavelength. Moreover, the transmission bandwidth of the measured

peak (appeared due to phase-shift keying) is less than 0.1 nm. This result reinstates the advantage of the phase-shift keying technique to produce a narrower bandwidth filters with shorter gratings. The multi-channel filter corresponds to more than one equidistant

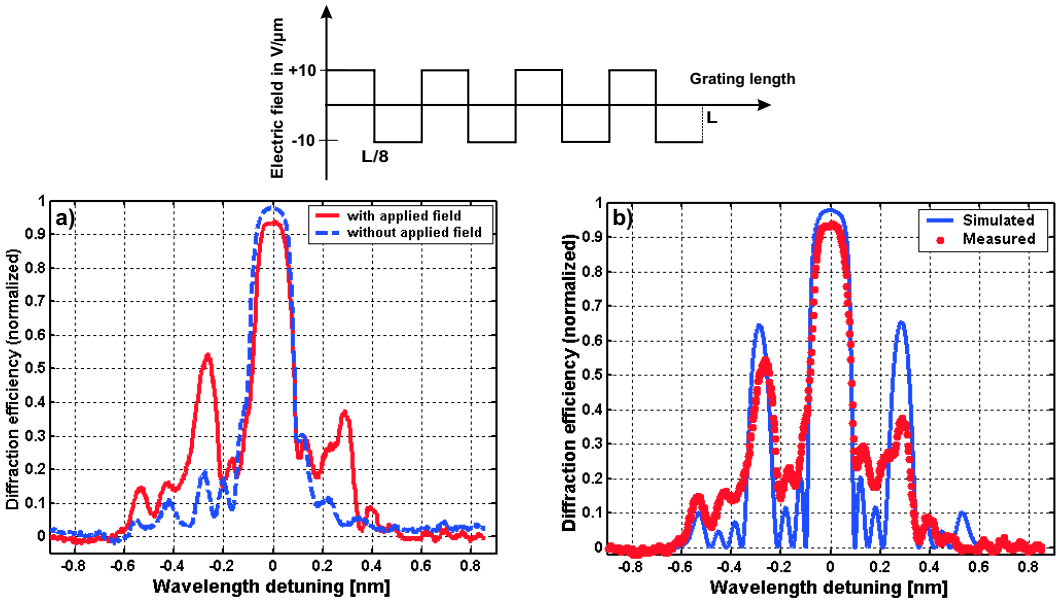

Figure 6.9: Synthesis of a three channel filter with electro-optically applied phase-shift scheme as shown above the plots: a) Measured transfer function of the grating filter without (dashed) and with (solid) applied electric field and b) experimentally measured (filled circles) with theoretically simulated (solid) transfer function.

channels. Fig. 6.9 shows the synthesized transfer function for a three channel filter. The corresponding phase-shift keying scheme is shown over the plots. Electric fields of equal magnitude and opposite polarity were applied on alternative electrodes and such a scheme resulted in a three channel filter. A comparison with the theoretically simulated result confirms the measurements as the positions of the peaks match. As the grating is not very homogeneous, one of the measured peaks is not nicely resolved. Another point to mention is that the maximum value of the field that could be applied did not induce a phase-shift necessary to produce three peaks of equal strength as discussed in [133]. The measured result, however, verifies the concept of electro-optical phase-shift keying for synthesizing multi-channel filters.

A five-channel filter was synthesized next as shown in Fig. 6.10. The corresponding phase-shift keying scheme is also shown in the figure. Electric field of equal magnitude and opposite polarity was applied on alternative pairs of electrodes. The measured result was compared with the theoretical result calculated using the phase-shift keying applied for the measurement. The experimentally measured data fits well to the theory except one peak which was not nicely resolved due to the internal phase errors of the grating. The spectral separation between the peaks was 0.14 nm. Apart from the demonstrated transfer

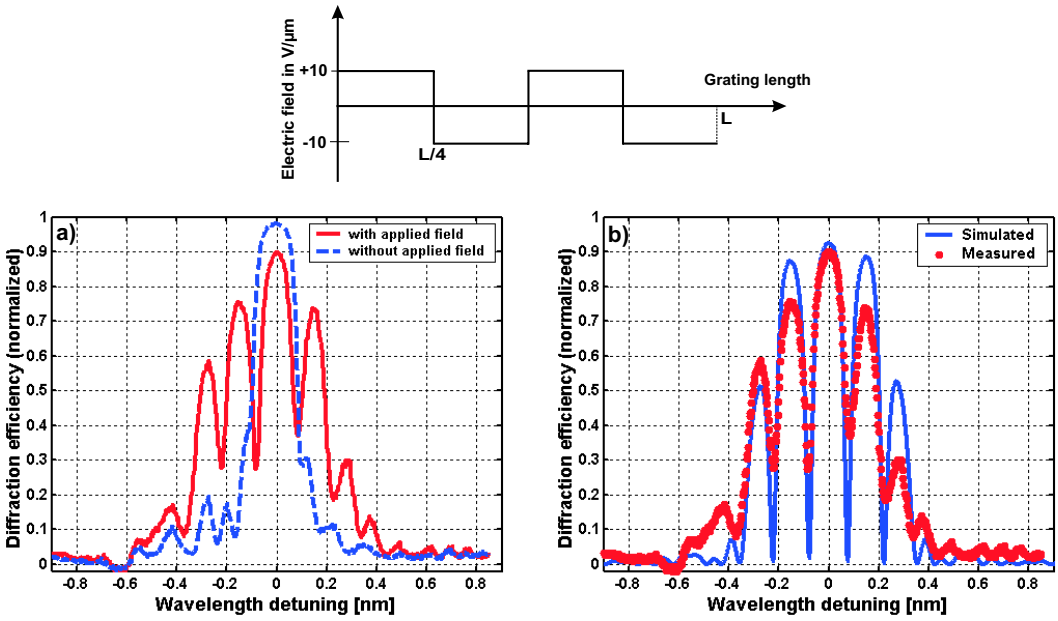

Figure 6.10: Synthesis of a five channel filter with electro-optically applied phase-shift scheme as shown above the plots: a) Measured transfer function of the grating filter without (dashed) and with (solid) applied electric field and b) experimentally measured (filled circles) with theoretically simulated (solid) transfer function.

functions for the multi-channel filters, there are more reconfiguration possible such as six or seven channel filter. Due to the limited number of electrodes and a limited value of the applied electric field, more reconfigurations for multi-channel filters could not be nicely resolved. A better electrode geometry and larger number of cells will allow a more effective manipulation of the phase profile in an even wider variety.

6.4.3 Flat Top Transfer Function

A flat top transfer function has a broad and flat reflection peak. In many cases, a flat-top filter transfer function with steep edges is required in communication networks. Such a filter profile is used to filter a certain spectrum of more than one neighboring channels with the same efficiency. A flat-top is also a single peak transfer function and its profile depends on the grating amplitude and the length for the case of uniform gratings. However, phase-shift keying can be efficiently applied to generate such a profile even for low grating amplitudes [133]. The investigated gratings exhibited high diffraction efficiencies though. The synthesized flat top transfer function is shown in Fig. 6.11. The actual voltage applied to each electrode is also mentioned in the figure. Comparing with the original transfer function, the synthesized transfer function has a considerably broadened and flattened peak and the edges are steeper. The flat-top peak is shifted with respect to the position

of the peak in the original transfer function and this is due to some internal phase-errors in the grating. As the grating is apodized, sidelobes are also suppressed as can be seen in the figure. The quality of the profile, however, can be further improved with an additional apodization and a better homogeneous profile of the grating amplitude.

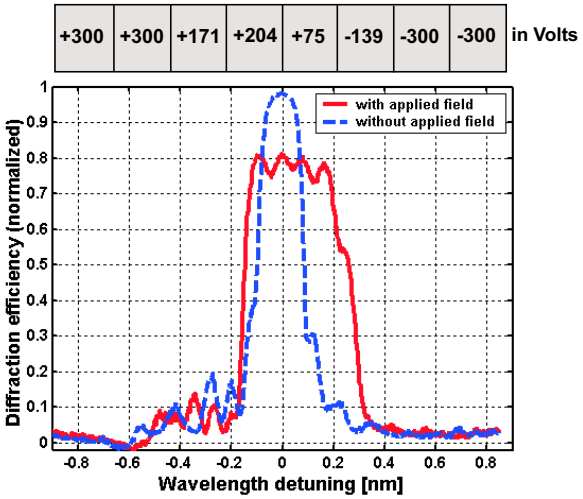

Figure 6.11: Synthesis of a flat top transfer function with the applied (phase-shift) voltage scheme as shown above the plot: measured transfer function of the grating filter without (dashed) and with (solid) applied electric field.

6.4.4 Dynamic Correction of the Transfer Function Profile

The technique of electro-optical phase-shift keying was further explored for a dynamic correction of the transfer function profile e.g. suppression of side lobes, suppression of undesired peaks appearing due to internal phase errors of the grating as shown in Fig. 6.12. The solid line represents the corrected profile and dashed line represents the original profile of the transfer function without any applied voltage. The actual voltage applied to each electrode is also shown in the figure. By applying a phase-shift via the applied voltage on different electrodes, unnecessary peaks seen in the transfer function profile occurring due to internal phase errors of the grating can be compensated. As can be seen, the small kink appearing on the longer wavelength side of the main peak of the original transfer function was removed after the phase-shift keying scheme was applied. In doing so, the sidelobes could also be suppressed which is often required in communication systems in order to reduce cross-talk. However, the central peak of the corrected profile shifts to the lower wavelength side by the applied phase-shifts. Nevertheless, the smoother transfer function profile which comes at the cost of a wavelength shift of about 0.02 nm could be very interesting for many application. Apart from the one reconfiguration shown here, many other corrections can be done to the profile just by varying the phase-shift in each grating section which is done by varying the voltage applied to each electrode pair.

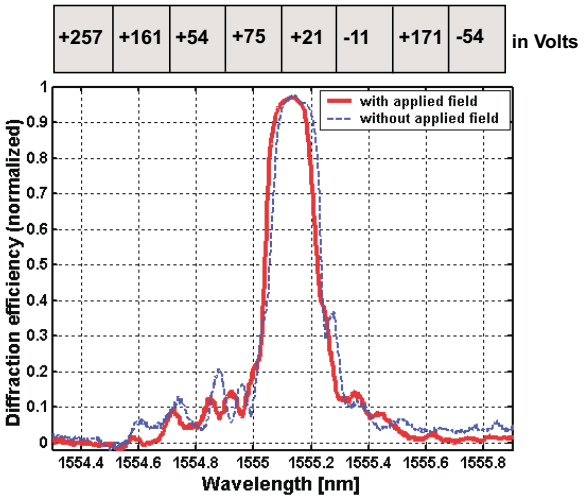

Figure 6.12: Dynamic correction of the transfer function with the applied (phase-shift) voltage scheme as shown above the plot: measured transfer function of the grating filter without (dashed) and with (solid) applied electric field.

The bandwidth and the shape of the transfer function can also be controlled to some extent via electro-optical phase-shift keying. As shown in Fig. 6.13(a) and (b), changing the phase-shift keying can make the peak narrower or broader than in the original transfer function. The solid line represents the original transfer function and the other two transfer functions are synthesized via phase-shift keying as mentioned in the figure. For Fig. 6.13(b), a linear phase-shift keying (increasing or decreasing phase-shifts for successive sections) was used. Using such a scheme introduces a chirp in the grating leading to

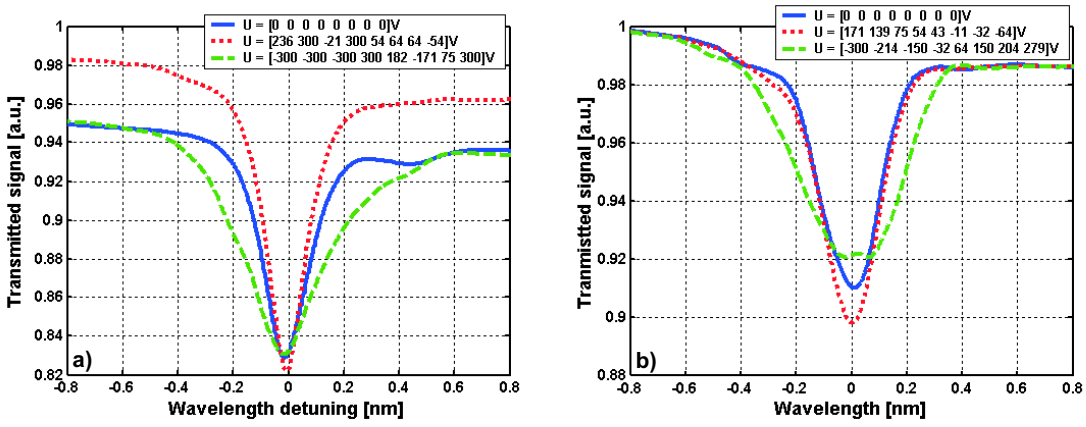

Figure 6.13: a) and b)Dynamic control of the shape of the transfer function with the applied (phase-shift) voltage schemes: measured transfer function of the grating filter without (solid) and with (dashed) applied voltage schemes.

compression or expansion of the signal. Inclusion of chirped gratings is a common practice especially in fiber Bragg gratings used for dispersion compensation applications. The technique I proposed is also promising for dispersion compensation applications where an incoming signal needs to be compressed in order to compensate for the dispersion. The advantage of the proposed technique is that a grating can be dynamically and virtually chirped without actually fabricating a grating with chirped grating period.

6.5 Switching Time Analysis

The electro-optical phase-shift keying provides dynamical control of the transfer function for the single fabricated grating filter. The reconfigurations shown in the previous section demonstrate the potential of this technique. It is, however, important to consider the switching time which in this case is defined as the time required to switch from one reconfiguration to the other. Potentially, this time should be in the nanosecond regime considering the nature of the electro-optical control and the integrated optical implementation (reduction of the dimensions). A switching time analysis was performed for measuring the time required for switching between two single channels as shown in Fig. 6.7 (b). The maxima of one channel falls on the minima of another channel by applying $\pm$ 300 Volts. Therefore, a square pulsed ac voltage with peak-to-peak voltage of 300 Volts and a frequency of 50 kHz was applied to all the electrode pairs. The laser was fixed at the central wavelength of the original transfer function without application of the external voltage to the electrodes and the transmitted signal was measured with time using the National Instrument's analog input-output card via a Labview program. For half of the duration of the square pulse cycle, the applied voltage was zero and so the transmitted signal was zero as most of the power is reflected at the selected wavelength. For the other half duration of the pulse, the voltage was 300 V and so the transmitted signal was maximum as the selected wavelength in not reflected anymore. The measured response of the transmitted signal also followed a square wave profile after the applied voltage pulse as shown in Fig. 6.14(b). Fig. 6.14(c) shows the magnified version of Fig. 6.14(b). However, the applied voltage takes some time to affect the transmission signal and this can be noticed as the rise and fall of the wave in the measured signal is not sharp (Fig. 6.14(c)) like the input pulse (Fig. 6.14(a)). This delay in the measured signal for reaching from maximum to minimum value or vice-versa determines the switching time, which was estimated as 1 μs. This time was, however, limited by the resolution of the input-output card. This means that actual switching time is even less than 1 μs.

Another experiment was performed in order to confirm the switching time. Signals from two tunable IR lasers were coupled via a 3-dB coupler to the input port of the realized grating filter. The signal from one laser was fixed at the central wavelength of the reflection filter. The signal from the other laser was fixed at a wavelength to which the filter switched on application of 300 V (or +10 V/μm) on all the electrodes (as shown in Fig. 6.7(b))

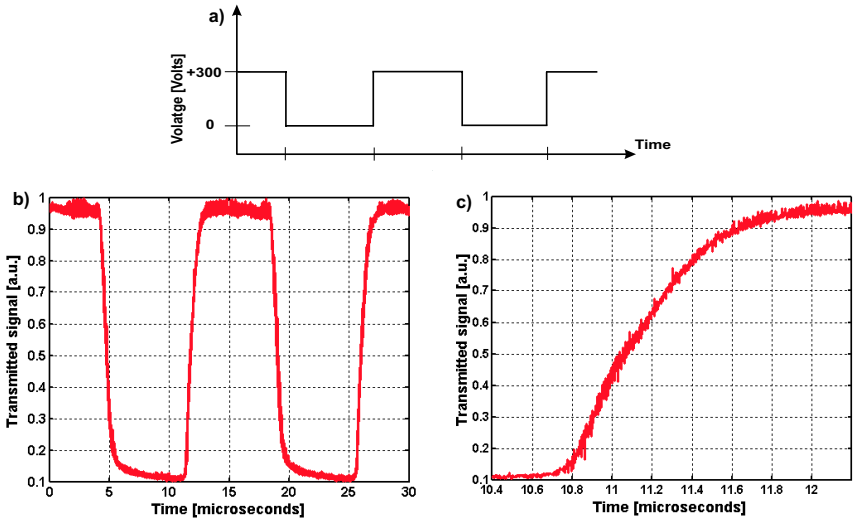

Figure 6.14: Switching time analysis: a) the input square voltage pulse; b) the measured transmitted signal as a function of time; c) magnified version of b).

and this signal had either a power (Fig. 6.15(a)) different from the other signal or was modulated with additional noise (Fig. 6.15(b)). The same square voltage pulse as shown in Fig. 6.14(a) was then applied to the filter and the transmitted signal was measured with time as shown in Fig. 6.15. For half of the square pulse, one wavelength is completely reflected and for another half of the cycle, the other wavelength is completely reflected. The switching between two channels was achieved with a switching time of 1 μs and this result confirms the value of switching time. This is definitely an improvement from switching time for the bulk implementation as discussed in Chapter 4 which was in the range few hundred microseconds. This was expected as the dimension are reduced and the voltage

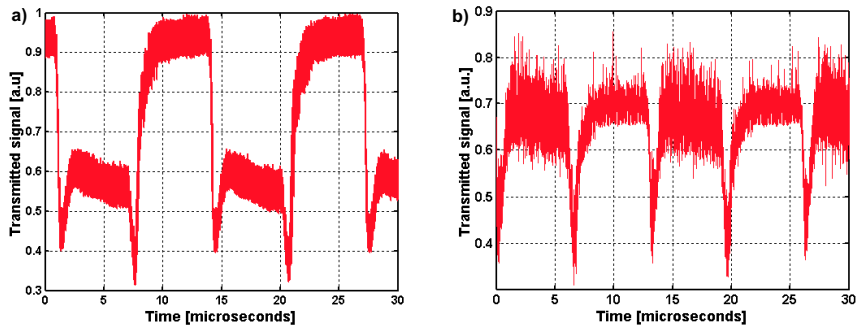

Figure 6.15: Switching time analysis: a) measured transmitted signal as a function of time for switching between two channels with different power or strength; b) measured transmitted signal as a function of time for switching between two channels with one of the channels modulated with additional noise.

requirement is also reduced compared to the system examined in chapter 4. The switching speed in few hundred GHz range reinstates the advantage of electrical control and makes such a filter more dynamic and useful for various high-speed applications.

6.6 Potential Applications

Based on the results obtained with electro-optical phase-shift keying as presented in this chapter, there can be some very promising applications for grating based integrated optical filter with fast reconfigurable transfer function. The continuous tunable single channel filter with fast speed and wavelength accuracy even within a relatively narrow spectral range could be interesting for wavelength locking and stabilization of lasers based on the principles discussed in [150–152]. The multi-channel filter reconfiguration could be interesting for applications which require a spectral selection and control of many discrete channels in broad wavelength range. Moreover, several such integrated gratings with different central reflection wavelengths can be either fabricated on the same substrate or on different substrates which can be joined using optical fibers. The reflectivity of each grating can be independently controlled by applying appropriate spatial distribution of the electric field. An array of such gratings can be used for realizing electrically controllable multiplexers, modulators, optical attenuators etc. Another important feature of the realized grating filter is fast dynamical control due to the electro-optical nature of the control. With such device, discrete wavelength channels can be controlled with very high speed (few hundred GHz or faster). The array of such electrically controllable gratings can be used for independent modulation of each channel. Conventional DWDM systems contain a large number of narrowband stable lasers with external modulators, which makes the system complicated and expensive. The proposed array of electrically controlled integrated gratings can be used with a broadband ASE source and can act as a wavelength multiplexer. Moreover, the gratings will also act as high frequency optical modulator. Such a proposed technique could be very useful for DWDM systems for making them simple and cost-effective.

Integrated optical Bragg gratings with fast electrical control can be very interesting also for OCDMA networks which need reconfigurable devices. The proposed integrated Bragg gratings can replace the fiber Bragg gratings as discussed in [127] to act as fast encoder/decoder for OCDMA networks. Apart from this, the filter can be used as an add-drop filter with favorably reconfigurable transfer function. Moreover, such narrow-band filters may also find applications in spectroscopy.

Chapter 7

Summary and Outlook

This last chapter aims to summarize the previous chapters with a special emphasis on the primary results achieved during the work. In addition, an outlook is presented at the end of the chapter to provide a basis for further investigations and applications.

7.1 Summary

Bragg gratings due to their inherited property of narrow-band spectral filtering, infiltrated almost all applications in optical communication networks. With the evolution of the dynamically reconfigurable communication networks, Bragg grating also needs to evolve as a fully reconfigurable and tunable device. This dissertation emphasizes on the realization, investigation and manipulation of Bragg gratings with external electrical control especially for spectral filtering applications. Volume photorefractive Bragg gratings were realized in bulk lithium niobate crystals and were manipulated with external electric field in order to demonstrate fast electrically switchable lenses and mirrors. Photorefractive Bragg gratings were then inscribed in lithium niobate waveguides and a fast electrically tunable integrated optical spectral filter was demonstrated. In addition, a detailed investigation of higher harmonic components of nonlinear photorefractive waveguide gratings in reflection geometry has been performed for the first time to the best of my knowledge.

The most important and interesting part of the entire work was the introduced concept of phase-shift keying of corrugated waveguide Bragg gratings which was used to dynamically reconfigure the filter transfer function. This novel concept comprises, for the first time to the best of my knowledge, the use of external electric field to dynamically inscribe phase-shifts to more than two sections of the already fabricated integrated corrugated Bragg grating. Employing this technique, a fast ($< 1\ \mu$s) reconfiguration or synthesis of the transfer function into several desirable profiles was demonstrated. The term transfer function was used to describe the spectral dependence of diffraction efficiency and it

contains information about the amplitude and phase-modulations of the original grating. This function can be obtained by illuminating the grating with a tunable infrared laser and measuring the transmitted or the reflected signal as a function of the wavelength.

The thesis begins with a discussion on the theoretical framework on diffraction analysis of volume Bragg gratings with a special emphasis on reflection Bragg gratings. Throughout this work, Bragg gratings were read-out in reflection and it was important to know the influence of grating length, grating period, coupling strength, and deviations from the Bragg condition on the diffraction characteristics of the grating. Kogelnik's coupled wave theory was discussed in detail in chapter 2 to make a common base for the Bragg gratings discussed in following chapters. Based on the coupled wave theory analysis, the high wavelength selectivity offered by reflection gratings is widely used for multiplexing holograms in volume in order to increase the capacity and the functionality. This refractive index selectivity is equivalent to the spectral selectivity and thus the reflection geometry is best also for the electric-field multiplexing.

The basic understanding of the photorefractive effect was necessary before proceeding to the realization of photorefractive gratings. The most widely accepted band-transport model and the underlying charge transport mechanisms were discussed in chapter 3. In addition, the effect of the photovoltaic field on the grating formation was discussed specifically for lithium niobate. As the goal was to realize electrically controllable optical Bragg gratings, the material used for all the investigations was $LiNbO_3$ due to its outstanding optical and electro-optical properties. In addition, excellent photorefractive properties of $LiNbO_3$ make it suitable for the realization of refractive-index Bragg gratings. Moreover, $LiNbO_3$ bulk single crystals are readily available and waveguide fabrication techniques available for this material are well-established.

Electrical control of diffraction from volume photorefractive gratings in bulk Fe:$LiNbO_3$ crystal was tested initially. Photorefractive volume gratings were multiplexed using electrical field multiplexing (EFM) in order to realize electrically switchable holographic lenses and mirrors. For reducing the voltage requirements and for using the electrical control efficiently, the experimental geometry and the crystal orientation was optimized based on detailed analytical calculations as presented in chapter 4. In order to optimize the electric field selectivity (EFS), the grating period should be small and the length should be large and this encouraged to use the reflection geometry for recording as well as for read-out. Furthermore, transverse configuration of the electro-optic effect was used in order to reduce the voltage requirements. The crystal orientation was optimized considering the dependence of effective electro-optic coefficient and the grating amplitude on the angle α between the $\overrightarrow{C}$-axis and the applied electric field. An optimal value of α was found to be 45° for the case of extra-ordinary polarization. Four samples of iron doped lithium niobate crystals with 0.05 mol% concentration of Fe^{2+} ions and with dimensions 10 mm x 8 mm x d mm were used, where d = 1, 1.5, 2.5, and 5. The value of EFS was measured to be $\pm$ 2 kV/cm. This value was further used to multiplex holograms using the Rayleigh's criterion. Holograms of two lenses with 40 cm and 60 cm focal length were multiplexed at

two different values of the applied field. During read-out, light was focussed at 40 cm or 60 cm by switching the value of the applied field. Thus, I could realize a holographic lens with electrically switchable focal length.

In the next step, holograms of mirrors were recorded and multiplexed at two different values of the applied electric field. The same mirror at two different orientations was used for two recordings. This was actually a combination of angular and electric field multiplexing. During read-out, the direction of the reconstructed beam was switched by switching the value of the applied field. The angular deflection between the two beam reconstructed on electrical switching was $50°32'$. Here, a holographic mirror was realized with electrical switching of direction. A switching time analysis was then performed to measure the time taken for switching between two holograms. The crystal between the electrodes acts as a capacitor and limited the switching time to 100 μs. Chapter 4 ends with a conclusion that when used for integrated optical dimensions, the electrical control could be much faster.

From chapter 5 onwards, electrical control of diffraction has been discussed for waveguide gratings. A short review of the waveguide theory, coupling techniques and coupled-wave theory of waveguide Bragg gratings was discussed in the beginning of chapter 5. Two types of waveguide Bragg gratings (photorefractive and photolithographic or corrugated) were realized and discussed in detail. A photorefractive index grating was first recorded in a Ti:$LiNbO_3$ waveguide with a period of about 350 nm in order to filter telecommunication wavelengths when read-out in reflection. Such an integrated optical filter based on photorefractive waveguide gratings exhibited high diffraction efficiency (more than 90%) and narrow-bandwidth (0.16 nm) of the filter transfer function centered at a wavelength near 1555 nm. The measured results fitted nicely to the theoretically predicted results based on Kogelnik's theory. On application of an external electric field to thin film electrodes deposited on both sides of the waveguide grating, the transfer function could be continuously tuned. The total tuning range for an applied electric field between ± 4.8 V/μm was 0.14 nm. During our experiments, the used modulation depth was near 1 and the inscribed gratings exhibited high diffraction efficiency for the fundamental harmonic. Therefore, these gratings were further investigated for nonlinear properties. The diffraction from higher nonlinear harmonics of photorefractive gratings was observed in reflection geometry, for the first time to the best of my knowledge. The observation of significant diffraction from second and third harmonic components as reported by this study are interesting and important for all the applications based on photorefractive reflection gratings.

Corrugated or surface-relief Bragg gratings were next realized in Ti:$LiNbO_3$ waveguide. These gratings offer the advantage of being permanent unlike their photorefractive counterparts and are promising considering the possibility of mass-production. Various aspects of design of corrugated gratings were discussed to get the initial working parameters which were further optimized with repetitive fabrication and examination steps. The process of fabrication of corrugated gratings in lithium niobate was discussed in great detail including the discussion on challenges faced during the fabrication process and their solutions. An intensive literature survey has been included in order to provide a complete overview to the

reader. The holographically patterned grating in photoresist was transferred to the waveguide surface using reactive ion etching (RIE) with SF_6 gas. The chromium was deposited with a shadow evaporation technique over the photoresist grating to serve as a hard mask for the following RIE. Two different approaches to prepare a hard-mask were used and discussed. The crystal was then packed in a protective cover and single-mode fiber pigtails were attached to both ends of the waveguide. The measured transfer function exhibited a narrow bandwidth (0.17 nm), a central wavelength near 1555 nm and a continuous tuning of the filter transfer function with the applied external field. The experiments have shown a continuous tuning of the central wavelength in the range 0.3 nm with a maximum applied field of ± 10 V/μm. Such an integrated optical filter based on corrugated gratings with a continuously tunable transfer function seem to be very promising for DWDM applications as the measured bandwidth of 0.17 nm is four times better than the interchannel spacing of 0.8 nm required in present DWDM networks.

In the next step, the functionality of electrically tunable integrated Bragg gratings was extended using the introduced electro-optical phase-shift keying. With this novel technique, instead of applying a homogeneous electric field as was done for tuning the transfer function, a spatial distribution of the applied electric field leads to spatial distribution of the refractive index ultimately leading to a phase distribution over the structure, which is nothing but phase-shift keying. Here, an already fabricated corrugated waveguide grating, as discussed in chapter 5, was used. However, instead of a single electrode pair over the grating length, the single electrode pair was split into 8 separate independent electrode pairs. The length of each grating section was about 1 mm and the separation between neighboring electrodes was about 50 μm. By applying different combinations of electrical voltages to different electrodes, a different amount of phase-shift can be induced to each grating section and by doing this, the spectral transfer function can be tailored (or reconfigured or synthesized). As the electro-optic effect is exploited for inducing phase-shifts, the name electro-optical phase-shift keying was introduced by me.

Chapter 6 introduced various aspects of this phase-shift keying technique. The basic principle of phase-shift keying was explained and an extension of the coupled-wave theory for segmented (with different phases) Bragg grating was discussed. An overview of existing techniques used for the experimental implementation of the phase-shift keying was presented together with the detailed discussion on the electro-optical phase-shift keying. The biggest advantage of this technique is that one single homogeneous grating is used to exhibit dynamic and fast control of the transfer function. There are no mechanical movements required for reconfiguring the transfer function making this technique additionally fast and effective. Moreover, it offers a great deal of flexibility and dynamical control at the operational level as the induced phase-shifts are controlled by external voltage applied to the electrodes leading to real-time complex transfer function reconfigurations.

For the first time to the best of my knowledge, the use of external electric field to dynamically inscribe phase-shifts to more than two sections of the already fabricated integrated Bragg grating. Employing this technique, a fast (< 1 μs) reconfiguration or synthesis of the

transfer function was demonstrated. Some of the realized reconfigurations e.g. continuous tuning of a single selected channel, reconfiguration from pass-band to stop-band, reconfiguration from one to two, three and five pass-bands, reconfiguration to a flat-top profile, dynamic correction of the transfer function profile, dynamic control of the bandwidth and the shape of the transfer function are presented in chapter 6. For the synthesis of a desired transfer function profile, the desired phase-profile (voltage combination) was calculated based on the transfer matrix algorithm. There was an excellent agreement between most of the experimentally realized transfer functions and those predicted by theoretical simulations. However, due to some phase-errors in the fabricated gratings, a satisfactory match was not found between the theoretically predicted and the realized transfer function in some cases e.g. for the case of flat-top profile of the transfer function. However, the proposed technique offers the advantage of real-time reconfiguration of the transfer function and due to this the dynamic corrections to the transfer function profile could be easily performed by just varying the voltage applied to different electrodes. This technique was also successfully used to demonstrate the real-time control of the transmission bandwidth. The proposed technique can be used to induce phase-shift to the grating in a way that it forms a chirped grating and could be used for dispersion compensation applications. One of the most promising results was the estimation of switching time. In my experiments, I was able to demonstrate switching with time less than 1 μs (few GHz). With such fast switching, the proposed integrated optical filters with reconfigurable transfer functions are very promising not only for the existing DWDM networks but also for the next generation high-speed reconfigurable telecommunication networks like OCDMA (optical code division multiple access).

7.2 Outlook

Various designs of Bragg grating based filters with a reconfigurable transfer function are being designed and developed by different groups of scientists. However, most of the emphasis of the research has been devoted on the development of the phase-shift keying techniques for fiber Bragg grating based filters. An integrated optical filter with a reconfigurable transfer function, as presented in my work, should trigger new impulses in the field of reconfigurable optical communication networks. The fast (few GHz) and dynamic control offered by the proposed technique makes it very promising for high-speed telecommunication applications. However, there is still a lot of scope for further development of the proposed technique. The tuning range achieved with the maximum applied voltage can be increased by choosing an advanced design and geometry of electrodes. A study on various electrode designs would be interesting in order to optimize the electrical control.

The synthesis of the transfer function was discussed in this study. However, the inverse problem of grating synthesis based on the observed transfer function can reveal basic grating properties such as grating amplitude and phase profile, coupling coefficient variation

over the length of the grating, dispersion characteristics, etc. Techniques like layer peeling [153] and inverse scattering algorithm [154] can be used to synthesize the Bragg gratings from the observed transfer function. This study can provide an insight into the design and characterization of the gratings with complex profiles.

The proposed grating filter can be efficiently used for wavelength locking and stabilization of tunable lasers and some tests in this direction can lead to interesting results. Moreover, several integrated gratings with different central reflection wavelengths can be either fabricated on the same substrate or joined back to back on different substrates. The reflectivity of each grating can be independently controlled by applying an appropriate spatial distribution of the electric field. An array of such gratings can be used for realizing electrically controllable multiplexers, modulators, optical attenuators etc. Conventional DWDM systems contain a large number of narrowband stable lasers with external modulators, which makes the system complicated and expensive. The proposed array of electrically controlled integrated gratings can be used with a broadband ASE source and these can act as a wavelength multiplexer/demultiplexer. Moreover, the gratings will also act as high frequency optical modulator. Such a proposed technique could be very useful for DWDM systems making them simple and cost-effective.

Apart from the extension of the present work, some open questions about the applicability of the realized filters to the communication networks can be addressed. The proposed integrated Bragg gratings could be tested for replacement of the fiber Bragg gratings as discussed in [127] to act as fast encoder/decoder for OCDMA networks. I am confident that the presented results can generate new impulses and ideas in the field of optical filters and other fields as well.

Appendix: Material Properties of $LiNbO_3$

This section intends to give an overview of the basic material properties of $LiNbO_3$. A brief introduction in the beginning asserts on the aptness of this material for the presented investigations.

Lithium niobate is a versatile material being used widely in optical, acoustic and integrated devices. It is one of the most thoroughly characterized electro-optic materials, and since 1965 when Ballman reported the successful growth of single crystals by the Czochralski technique, intensive study on $LiNbO_3$ has been done [1,2]. Czochralski-grown monocrystals have unique electro-optical, piezoelectric, photoelastic and nonlinear optical properties. They are strongly birefringent. They are used in laser frequency doubling, nonlinear optics, Pockels cells, optical parametric oscillators, Q-switching devices for lasers, other acousto-optic devices, optical switches for gigahertz frequencies, etc.

$LiNbO_3$ is a colorless solid with trigonal structure and belongs to the point-symmetry group 3m. Its melting point is 1257°C and its density is 4.65 g/cm^3. It is a hard dielectric with Mohs hardness 5. It is generally available in pure form. However, the structure of $LiNbO_3$ can accommodate a large number of defects so that very large space-charge fields, and thus large refractive index gratings can build up. Commonly used dopants are Fe, Cu, Mg, Ti, Er, and Mn. The photoconductivity is generally small and so the photorefractive response time of lithium niobate is very slow, often exceeding several minutes. It has a low dark conductivity and so it can store holograms for a long time and therefore, it is suitable for holographic storage and long-term applications. In addition, lithium niobate is a very important electro-optic material due to its high electro-optic coefficients. The electro-optic tensor is of rank 3 and due to the symmetry of point group 3m, there are only eight non-zero and four independent electro-optic coefficients as shown in the electro-optic tensor (in compressed notation) [3],

$$[\hat{r}] = \begin{pmatrix} 0 & -r_{22} & r_{13} \\ 0 & r_{22} & r_{13} \\ 0 & 0 & r_{33} \\ 0 & r_{51} & 0 \\ r_{51} & 0 & 0 \\ -r_{22} & 0 & 0 \end{pmatrix}$$

where, $r_{13} = 8.6pm/V$, $r_{22} = 3.4pm/V$, $r_{33} = 30.8pm/V$, and $r_{51} = 28pm/V$. Moreover, its electro-optic properties have also been tested under extremely high external electric fields of up to 65kV/mm [4,5,6]. Furthermore, $LiNbO_3$ doped with Iron (Fe) and Copper (Cu) has a high photorefractive sensitivity [7]. It is an excellent material to manufacture optical waveguides with well-established fabrication techniques. Considering these arguments, $LiNbO_3$ is a suitable material for my investigations as I have used the photorefractive properties of this material for the recording of Bragg gratings in bulk and channel waveguides as well as the electro-optical properties for switching and tuning applications. The specifications of the crystals used during my investigation has been included in the earlier chapters. Some of the basic optical properties of $LiNbO_3$ are summarized in the following table[1].

Optical Symmetry	Negative Uniaxial
Transparency Range	420-5200 nm
Optical Absorption Coefficient	$\sim 0.1\%/cm@1064nm$
Optical Homogeneity	$\sim 5 \times 10^{-5}/cm$
Refractive Indices	$n_e = 2.156, n_o = 2.232@1064nm$ $n_e = 2.203, n_o = 2.286@632.8nm$ $n_e = 2.231, n_o = 2.326@532nm$
NLO Coefficients	$d_{33} = 34.4pm/V$ $d_{33} = d_{15} = 5.95pm/V$ $d_{22} = 3.07pm/V$
Electro-optic Coefficients	$r_{13}^T = 10pm/V, r_{13}^S = 8.6pm/V$ $r_{22}^T = 6.8pm/V, r_{22}^S = 3.4pm/V$ $r_{33}^T = 32.2pm/V, r_{33}^S = 30.8pm/V$ $r_{51}^T = 32pm/V, r_{51}^S = 28pm/V$
Half-Wave Voltage, DC	3.03 kV (Electrical field $\parallel$ z, light $\perp$ z) 4.02 kV (Electrical field $\parallel$ x or y, light $\parallel$ z)
Damage Threshold	$100MW/cm^2(10ns, 1064nm)$

where T: high frequency measurements, S: low frequency measurements

References:

[1] Ed by: E. Kaldis, *Current Topics in Material Science, Volume I*, North-Holland Publishing Company, 1978.

[2] Ed by: K.K. Wong, *Properties of Lithium Niobate*, Inspec, United Kingdom, 2002.

[3] P. Yeh, *Introduction to Photorefractive Nonlinear Optics*, John Wiley & Sons., 1993.

[4] M. Luennemann, K. Buse, and B. Sturman, J. Appl. Phys. 94 (10), 6274 (2003).

[5] M. Luennemann, U. Hartwig, G. Panotopoulos, and K. Buse, Appl. Phys. B 76, 403 (2003).

[6] R. De Vre´, M. Jeganathan, J.P. Wild, and L. Hesselink, Opt. Lett. 19 (12), 910 (1994).

[7] M.P. Petrov, A.V. Chamrai, A.S. Kozlov, and I.V. Il'ichev, Tech. Phys. Lett. 30, 120 (2004)

Bibliography

[1] M.C. Hutley. *Diffraction Gratings*. Academic Press, London, 1982.

[2] Max Born and Emil Wolf. *Principles of Optics*. Cambridge University Press, 2003.

[3] W.L. Bragg, *The diffraction of short electromagnetic waves by a crystal*, Proc. of Cambridge Philosophical Soc. **17**, 43–57 (1914).

[4] K.O. Hill, Y. Fuiji, D.C. Johnson and B.S. Kawasaki, *Photosensitivity in optical fiber waveguides: application to reflection fibre fabrication*, Appl. Phys. Lett. **32**, 647–649 (1978).

[5] M.P. Petrov, S.I. Stepanov and A.A. Kamshilin, *Light diffraction in photorefractive ferroelectrics*, Ferroelec. **21**, 631 (1978).

[6] M.P. Petrov, S.I. Stepanov and A.A. Kamshilin, *Light diffraction from the volume holograms in electro-optic birefringent crystals*, Opt. Comm. **29**, 44 (1979).

[7] P. Boffi, D. Piccinin and M.C. Ubaldi. *Infrared Holography for Optical Communications*. Springer, 2003.

[8] V.M. Petrov, S. Lichtenberg, J. Petter, T. Tschudi, A.V. Chamrai, V.V. Bryskin and M.P. Petrov, *Optical on-line controllable filters based on photorefractive crystals*, J. Opt. A: Pure Appl. Opt. **5**, s471 (2003).

[9] A. Locco, H.G. Limberger and R.P. Salathe, *Bragg grating fast tunable filter*, Elect. Lett. **33**, 2147 (1997).

[10] J.Y. Liu and K.M. Johnson, *Analog smectic c^* ferroelectric liquid crystal fabry perot optical tunable filter*, IEEE Phot. Technol. Lett. **7**, 1309 (1995).

[11] E. C. Vail, M.S. Wu, G. S. Li, L. E. Eng and C. J. Chang-Hasnain, *GaAs micromachined widely tunable fabry perot filters*, Elect. Lett. **31**, 228 (1995).

[12] H. Herrmann, K. Schafer and C. Schmidt, *Low loss tunable integrated acoustooptical wavelength filter in $LiNbO_3$ with strong sidelobe suppression*, IEEE Phot. Technol. Lett. **10**, 120 (1998).

[13] H. Kogelnik, *Coupled wave theory for thick hologram gratings*, Bell System Tech. J. **48**, 2909 (1969).

[14] L. Solymar and D.J. Cooke. *Volume Holography and Volume Gratings*. Academic Press, 1981.

[15] R.J. Collier, C.B. Burckhardt and L.H. Lin. *Optical Holography*. Academic Press, 1982.

[16] D. Gabor, *Microscopy by reconstructed wavefronts*, Nature **161**, 777 (1948).

[17] P.K. Rastogi. *Holographic Interferometry:Principles and Methods*. Springer, 1994.

[18] N. George and J.W. Matthews, *Holographic diffraction gratings*, Appl. Phys. Lett. **9**, 212 (1966).

[19] A.K. Ghatak and K. Thyagarajan. *Optical Electronics*. Cambridge University Press, 2003.

[20] F.H. Mok, *Angle-multiplexed storage of 5000 holograms in lithium niobate*, Opt. Lett. **18**, 915–917 (1993).

[21] G.A. Rakuljic, V. Leyva and A. Yariv, *Optical data storage by using orthogonal wavelegth-multiplexed volume holograms*, Opt. Lett. **17**, 1471–1473 (1992).

[22] M.P. Petrov, A.V. Shamray and V.M. Petrov, *Spectral and electric field multiplexing of volume holograms and the potential of these techniques for holographic memory*, Opt. Memory and Neural Networks **7**, 19 (1998).

[23] C. Denz, G. Pauliat, G. Roosen and T. Tschudi, *Volume hologram multiplexing using a deterministic phase-encoding method*, Opt. Comm. **85**, 171–176 (1991).

[24] M.P. Petrov, A.V. Shamray, V.M. Petrov, and J. Sanchez-Mandragon, *Electric-field sensitivity of reflection volume holograms in $LiNbO_3$*, Opt. Comm. **153**, 305 (1998).

[25] V.M. Petrov, C. Denz, A.V. Shamray, M.P. Petrov and T. Tschudi, *Electric field selectivity and multiplexing of volume holograms in $LiNbO_3$*, Appl. Phys. B **71**, 43 (2000).

[26] V.M. Petrov, C. Denz, A.V. Shamray, M.P. Petrov and T. Tschudi, *Electrically controlled volume $LiNbO_3$ holograms for wavelength demultiplexing systems*, Opt. Mat. **18**, 191 (2001).

[27] J.V. Alvarez-Bravo, R. Mueller and L. Arizmendi, *Electric-field multiplexing of volume holograms in $linbo_3$*, Europhys. Lett. **31**, 443–448 (1995).

[28] N.V. Kuktharev, V.B. Markov, S.G. Odulov, M.S. Soskin and L. Vinetskii, *Holographic storage in electrooptic crystals I*, Ferroelec. **22**, 949 (1979).

[29] P. Yeh. *Introduction to Photorefractive Nonlinear Optics*. John Wiley and Sons, 1993.

[30] F.T.S. Yu and S. Yin. *Photorefractive Optics*. Academic Press, 2000.

[31] P. Günther and J.P. Huignard. *Photorefractive Materials and their Applications I*. Springer-Verlag, 1988.

[32] P. Günther and J.P. Huignard. *Photorefractive Materials and their Applications II*. Springer-Verlag, 1989.

[33] M.P. Petrov, S.I. Stepanov and A.V. Khomenko. *Photorefractive Crystals in Coherent Optical Systems*. Springer-Verlag, 1991.

[34] P. Günther. *Nonlinear Optical Effects and Materials*. Springer-Verlag, 2000.

[35] A. Ashkin, G.D. Boyd, J.M. Dziedzic, R.G. Smith, A.A. Ballman, J.J. Levinstein and K. Nassau, *Optically induced refractive index inhomogeneities in $LiNbO_3$ and $LiTaO_3$*, App. Phys. Lett. **9**, 72–74 (1966).

[36] F.S. Chen, J.T. LaMaccia and D.B. Fraser, *Holographic storage in lithium niobate*, Appl. Phys. Lett. **13**, 223 (1968).

[37] K. Shutter, J. Hullinger and P. Günther, *Photorefractive effects observed in the organic crystal $2-cyclooctylamino-5-nitropyridine$ doped with $7,7,8,8-tetracyanoquinodimethane$*, Solid State Commun. **74**, 867 (1990).

[38] S. Ducharme, J.C. Scott, R.J. Twieg and W.E. Moerner, *Observation of the photorefractive effect in a polymer*, Phys. Rev. Lett. **66**, 1846–1849 (1991).

[39] X. An, D. Psaltis and G.W. Burr, *Thermal fixing of 10,000 holograms in $LiNbO_3$:Fe*, Appl. Opt. **38** (1999).

[40] P. Hariharan. *Optical Holography: Principles, Techniques and Applications*. Cambridge University Press, 1996.

[41] C. Gu, Y. Xu, Y. Liu, J.J. Pan, F. Zhau and H. He, *Application of photorefractive materials in information storage, processing and communication*, Opt. Mat. **23**, 219–227 (2003).

[42] R.W. Boyd. *Nonlinear Optics*. Academic Press, 1992.

[43] J. Feinberg, D. Heiman, A.R. Tanguay and R.W. Hellworth Jr., *Photorefractive effects in light induced chagre migration in barium nitrate*, J. Appl. Phys. **51**, 1297 (1980).

[44] A.V. Chamrai, M.P. Petrov and V.M. Petrov, *Optical configuration for electric field multiplexing of volume holograms in photorefractive ferroelectrics*, OSA Trends in Optics and Photonics (TOPS) **27**, 515 (1999).

[45] A. Yariv and P. Yeh. *Optical Waves in Crystals*. John Wiley & Sons, 1984.

[46] M.Yu. Loktev, V.N. Belopukhov, F.L. Vladimirov, G.V. Vdovin, G.D. Love and A.F. Naumov, *Wave front control systems based on modal liquid crystal lenses*, Rev. Sci. Instrum. **71**, 3290–3297 (2000).

[47] A.F. Naumov, M.Yu. Loktev, I.R. Guralnik and G.V. Vdovin, *Liquid crystal adaptive lenses with modal control*, Opt. Lett. **23**, 992–994 (1998).

[48] P. Arora, V. Petrov, J. Petter and T.Tschudi, *Fast electrically switchable holographic mirrors*, OSA Trends in Optics and Photonics Series (TOPS) **99**, 750–755 (2005).

[49] F.R. Gfeller, *A colinear thin-film acousto-optic scanner*, J. Phys. D:Appl. Phys. **10**, 1833–1845 (1977).

[50] H. Urey, D.W. Wine and T.D. Osborn, *Optical performance requirements for mems-scanner based microdisplays*, Proc. of SPIE **4178**, 176–185 (1977).

[51] S.V. Kartaloupoulos. *Introduction to DWDM Technology*. SPIE Opt. Eng. Press and IEE press, USA, 2002.

[52] R.G. Hunsperger. *Integrated Optics*. Springer, 2002.

[53] A.W. Snyder and J. Love. *Optical Waveguide Theory*. Chapman and Hall, London, 1983.

[54] G. Lifante. *Integrated Photonics*. John Willey & Sons, 2003.

[55] Ed. by K.K. Wong. *Properties of Lithium Niobate*. INSPEC, United Kingdom, 2002.

[56] K. Takizawa, *Electro-optic cutoff modulator using a Ti-indiffused $LiNbO_3$ channel waveguide with asymmentric strip electrodes*, Opt. Lett. **11**, 818–820 (1986).

[57] D. Runde, S. Breuer and D. Kip, *Holographic reflection filters in photorefractive $LiNbO_3$ channel waveguides for applications as add/drop multiplexers*, OSA Trends in Optics and Photonics Series (TOPS) **99**, 772–776 (2005).

[58] C.E. Rüter, D.Runde and D. Kip, *Integrated optical sensor based on refractive index gratings in photorefractive $LiNbO_3$:Ti:Fe channel waveguide*, OSA Trends in Optics and Photonics Series (TOPS) **99**, 777–781 (2005).

[59] D. Brooks and S. Ruschin, *Integrated electrooptic multielectrode tunable filter*, J. Lightwave Tech. **13**, 1508–1513 (1995).

[60] D. Kip, *Photorefractive waveguides in oxide crystals: fabrication, properties, and applications*, Appl. Phys. B **67**, 131–150 (1998).

[61] P.K. Tien, R. Ulrich and R.J. Martin, *Modes of propagating light waves in thin deposited semiconductor films*, Appl. Phys. Lett. **14**, 291–294 (1969).

[62] M.L. Dakss, M. Kuhn, P.F. Heidrich and B.A. Scott, *Grating coupler for efficient excitation of optical guided waves in thin films*, Appl. Phys. Lett. **16**, 523–525 (1970).

[63] M. Kawachi, *Recent progress in silica-based planar lightwave circuits on silicon*, IEEE Proc. Optoelectron. **143**, 257–262 (1996).

[64] J.T. Boyd and S. Sriram, *Optical coupling from fibers to channel waveguides formed on silicon*, Appl. Opt. **17**, 895–898 (1978).

[65] B.C. Gibson, S.T. Huntington and J.D. Love, *Self-aligning method of fiber-to-waveguide pigtailing*, Opt. Lett. **30**, 2858–2860 (2005).

[66] A. Yariv and M. Nakamura, *Periodic structures for integrated optics*, IEEE J. of Quantum Elec. **13**, 233–253 (1977).

[67] J.E. Roman and K.A. Winick, *Neodymium-doped glass channel waveguide laser containing an integrated bragg reflector*, Appl. Phys. Lett. **61**, 2744–2748 (1992).

[68] S. Ura and S.J. Sheard, *A configuration for guided-wave excitation into a disposable integrated-optic head*, Opt. Comm. **146**, 85–89 (1998).

[69] D. Clerk and W. Lukosz, *Direct immunosensing with an integrated-optical grating coupler*, Sensors and Actuators **40**, 53–58 (1997).

[70] S. Fouchet, F.R. Ladan, F. Huet, A.Carenco, M. Carre and Y. Gao, *Ti-implanted bragg reflectors on $LiNbO_3$:Ti stripe waveguides*, Appl. Phys. Lett. **58**, 1518–1520 (1991).

[71] B.E. Benkelfat, R. Ferriere, B. Wacogne and P. Mollier, *Technological implementation of bragg grating reflectors in Ti:$LiNbO_3$ waveguides by proton exchange*, IEEE Phot. Tech. Lett. **14**, 1430–1432 (2002).

[72] M-C Oh, H-J Lee, M-H Lee, J-H Ahn, S.G. Han and H-G Kim, *Tunable wavelength filters with bragg gratings in polymer waveguides*, Appl. Phys. Lett. **73**, 2543–2545 (1998).

[73] A. Yariv, *Coupled-mode theory for guided-wave optics*, IEEE J. Quantum Elec. **9**, 919–933 (1973).

[74] A. Yariv and M. Nakamura, *Periodic structures for integrated optics*, IEEE J. of Quantum Elec. **13**, 233–253 (1977).

[75] T. Suhara and H. Nishihara, *Integrated optics components and devices using periodic structures*, IEEE J. of Quantum Elec. **22**, 845–867 (1986).

[76] Y. Yamamoto, T. Kamiya and H. Yanai, *Improved coupled wave analysis of corrugated waveguides and lasers*, IEEE J. of Quantum Elec. **14**, 245–258 (1978).

[77] T.E. Murphy. *Integrated optical grating based matched filters for fibre-optic communications*. Master's thesis, MIT, 1996.

[78] O. Parriaux, V.A. Sychugov and A.V. Tishchenko, *Coupling gratings as waveguide functional elements*, J. Opt. A:Pure Appl.Opt. **5**, 453–469 (1996).

[79] R. Müller, M.T. Santos, L. Arizmendi and J.M. Cabrera, *A narrow-band interference filter with photorefractive $LiNbO_3$*, J. Phys. D:Appl. Phys. **27**, 241–246 (1994).

[80] V. Leyva, G.A. Rakuljic and B. O'Conner, *Narrow bandwidth volume holographic optical filter operating at the Kr transition at 1547.82 nm*, Appl. Phys. Lett. **65**, 1079–1081 (1994).

[81] G.A. Rakuljic and V. Leyva, *Volume holographic narrow-band optical filter*, Opt. Lett. **18**, 459–461 (1993).

[82] R.T.B. James, C. Wah, K. Iizuka and H. Shimotahira, *Optically tunable optical filter*, Appl. Opt. **34**, 8230–8235 (1995).

[83] J. Hukriede, D. Runde and D. Kip, *Fabrication and application of holographic bragg gratings in lithium niobate channel waveguides*, J. Phys. D:Appl. Phys. **36**, R1–R16 (2003).

[84] J. Hukriede, I. Nee, D. Kip and E. Krätzig, *Thermally fixed reflection gratings for infrared light in $LiNbO_3$:Ti:Fe channel waveguides*, Opt. Lett. **23**, 1405–1407 (1998).

[85] J. Hukriede, D. Kip and E. Krätzig, *Permanent narrow-band reflection holograms for infrared light recorded in $LiNbO_3$:Ti:Cu channel waveguides*, Appl. Phys. B **72**, 749–753 (2001).

[86] Ch. Becker, A. Greiner, Th. Oesselke, A. Pape, W. Sohler and H. Suche, *Integrated optical Ti:Er:$LiNbO_3$ distributed bragg reflector laser with a fixed photorefractive grating*, Opt. Lett. **23**, 1194–1196 (1998).

[87] S. Breer and K. Buse, *Wavelength demultiplexing with volume phase holograms in photorefractive lithium niobate*, Appl. Phys. B **66**, 339–345 (1998).

[88] S. Breer, H. Vogt, I. Nee and K. Buse, *Low-crosstalk WDM by bragg diffraction from thermally fixed reflection holograms in lithium niobate*, Electron. Lett. **66**, 2419–2421 (1998).

[89] J. Hukriede, D. Kip and E Krätzig, *Investigation of titanium- and copper-indiffused channel waveguides in lithium niobate and their application as holographic filters for infrared light*, J. Opt. A:Pure Appl. Opt. **2**, 481–487 (2000).

[90] A.A. Freschi and J. Frejlich, *Adjustable phase control in stabilized interferometry*, Opt. Lett. **20**, 635–637 (1995).

[91] K. Peithmann, A. Wiebrock and K. Buse, *Incremental holographic recording in lithium niobate with active phase locking*, Opt. Lett. **23**, 1927–1929 (1998).

[92] M.P. Petrov, A.V. Chamrai, A.S. Kozlov and I.V. Il'ichev, *Electrically controlled integrated optical filter*, Tech. Phys. Lett. **30**, 120–122 (2004).

[93] M.G. Moharam and T.K. Gaylord, *Diffraction analysis of dielectric surface-relief gratings*, J.Opt. Soc. Am. **72**, 1385–1392 (1982).

[94] K. Yokomori, *Dielectric surface-relief gratings with high diffraction efficiency*, Appl.Opt. **23**, 2303–2310 (1984).

[95] M.G. Moharam, T.K. Gaylord, G.T. Sincerbox, H. Werlich and B. Yung, *Diffraction characteristics of photoresist surface-relief gratings*, Appl. Opt. **23**, 3214–3220 (1984).

[96] M.C. Gupta and S.T. Peng, *Diffraction characteristics of surface-relief gratings*, Appl. Opt. **32**, 2911–2917 (1993).

[97] M.G. Moharam and T.K. Gaylord, *Rigorous coupled-wave analysis of metallic surface-relief gratings*, J. Opt.Soc. Am. A **3**, 1780–1787 (1986).

[98] G. Niederer. *Resonant grating filters for microsystems.* Dissertation, Universite de Neuchatel, 2004.

[99] J.C. An, Y. Cho and Y. Matsuo, *Electrooptic-distributed bragg-reflection modulators for integrated optics*, IEEE J. Quant. Elec. **13**, 206–208 (1977).

[100] K. Chen, J. Ihlemann, P. Simon, I. Baumann and W. Sohler, *Generation of submicron surface-relief grating on $LiNbO_3$ by ultrashort UV pulses*, Appl. Phys. A **65**, 517–518 (1997).

[101] B. Wu, P.L. Chu, H. Hu and Z. Xiong, *UV-induced surface-relief gratings on $LiNbO_3$ channel waveguides*, IEEE J. Quant. Elec. **35**, 1369–1373 (1999).

[102] S. Mailis, G.W. Ross, L. Reekie, J.A.Abernethy and R.W. Eason, *Fabrication of surface relief gratings on lithium niobate by combined UV laser and wet etching*, Elec. Lett. **36**, 1801–1803 (2000).

[103] D.B. Ostrowsky and A. Jacques, *Formation of optical waveguides in photoresist films*, Appl. Phys. Lett. **18**, 556–557 (1971).

[104] F.W. Dabby, M.A. Saifi and A. Kestenbaum, *High-frequency cutoff periodic dielectric waveguides*, Appl. Phys. Lett. **22**, 190–191 (1973).

[105] R.C. Enger and S.K. Case, *Optical elements with ultrahigh spatial-frequency surface corrugations*, Appl. Opt. **22**, 3220–3228 (1983).

[106] M.J. Beesley and J.G. Castledine, *The use of photoresist as a holographic recording medium*, Appl. Opt. **9**, 2720–2724 (1970).

[107] W.T. Tsang and S. Wang, *Simultaneous exposure and development technique for making gratings on positive photoresist*, Appl. Phys. Lett. **24**, 196–199 (1974).

[108] C.V. Shank and R.V. Schmidt, *Optical technique for producing 0.1-μ periodic surface structures*, Appl. Phys. Lett. **23**, 154–155 (1973).

[109] D.P. Schinke, R.G. Smith, E.G. Spencer and M.F. Galvin, *Thin-film distributed-feedback laser fabricated by ion milling*, Appl. Phys. Lett. **21**, 494–496 (1972).

[110] F. Lacour, N. Courjal, M.P. Bernal, A. Sabac, C. Bainier and M. Spajer, *Nanostructuring lithium niobate substrate by focussed ion beam milling*, Opt. Mat. **27**, 1421–1425 (2005).

[111] S. Matsui, T. Yamato, H. Aritome and S. Namba, *Microfabrication of $LiNbO_3$ by reactive ion-beam etching*, Japanese J. Appl. Phys. **19**, L463–L465 (1980).

[112] B. Zhang, S. Forouhar, S.Y. Huang and W.S.C. Chang, *C_2F_6 reactive ion beam etching of $LiNbO_3$ and Nb_2O_5 and their application to optical waveguides*, J. Lightwave Tech. **2**, 7528–530 (1984).

[113] J. Soechtig, *Ti:$LiNbO_3$ stripe waveguide bragg reflector gratings*, Elect. Lett. **24**, 844–845 (1988).

[114] J. Soechtig, R. Gross, I. Baumann, W. Sohler, H. Schueltz and R. Widmer, *Dbr waveguide laser in erbium-diffusion-doped $LiNbO_3$*, Elect. Lett. **31**, 551–552 (1995).

[115] E.H. Anderson, C.M. Horwitz and H.I. Smith, *Holographic lithography with thick photoresist*, Appl. Phys. Lett. **43**, 874–875 (1983).

[116] P. Arora, V. Petrov, J. Petter and T. Tschudi, *Nonlinear properties of an integrated optical filter based on photorefractve gratings in $LiNbO_3$*, Frequenz **61**, 116–119 (2007).

[117] P. Arora, V. Petrov, J. Petter and T. Tschudi, *Detection of higher nonlinear harmonics of volume photorefractive gratings in reflection geometry*, Opt. Comm. **278**, 423–427 (2007).

[118] F. Vachss and L. Hesselink, *Nonlinear photorefractive resposne at high modulation depths*, J. Opt. Soc. Am. A **5**, 690 (1988).

[119] X. Chen, J. Zhao, R. Wang, X. Yi and P. Yeh, *Recording of second harmonic index gratings in photorefractive* $(K_{0.5}Na_{0.5})_{0.2}(Sr_{0.75}Ba_{0.25})_{0.9}Nb_2O_{46}$ *crystals*, Opt. Lett. **24**, 312 (1999).

[120] L.B. Au and L. Solymar, *Higher diffraction orders in photorefractive materials*, IEEE J. Quantum Elec. **24**, 162 (1988).

[121] Q.N. Wang, D.D. Nolte and M.R. Melloch, *Spatial-harmonic gratings at high modulation depths in photorefractive quantum wells*, Opt. Lett. **16**, 1944 (1991).

[122] B.L. Volodin, B. Kippelen, K. Meerholz, N.V. Kukhtarev, H.J. Caulfield and N. Peyghambarian, *Non-bragg orders in dynamic self-diffraction on thick phase gratings in photorefractive polymer*, Opt. Lett. **21**, 519 (1996).

[123] V.M. Petrov, S. Lichtenberg, J. Petter, T. Tschudi and A.V. Chamrai, *Adaptive interferometer with a femtometer-band resolution based on volume photorefractive holograms*, OSA Trends in Optics and Photonics (TOPS) **87**, 588 (2003).

[124] V.M. Petrov, C. Denz, A.V. Chamray, M.P. Petrov and T. Tschudi, *The effect of photovoltaic field on the bragg condition for the volume holograms in* $LiNbO_3$, Appl. Phys. B **72**, 701 (2001).

[125] B.I. Sturman and V. M. Fridkin. *The Photovoltaic and Photorefractive Effects in Noncentrosymmetric Materials*. Gordon and Breach Science Publishers, 1992.

[126] R. Goering, Z. Yuang-Ling and St. Steinberg, *Photoconductivity and photovoltaic behaviour of* $LiNbO_3$ *and* $LiNbO_3$ *waveguides at high optical intensities*, Appl. Phys. A **55**, 97 (1992).

[127] M.R. Mokhtar, M. Ibsen, P.C. Teh and D.J. Richardson, *Reconfigurable multilevel phase-shift keying encoder-decoder for all-optical networks*, IEEE Phot. Tech. Lett. **15**, 431–433 (2003).

[128] P.C. Teh, P. Petropoulos, M. Ibsen and D.J. Richardson, *A comparative study of the performance of seven- and 63-chip optical code-division multiple-access encoders and decoders based on superstructure fiber bragg gratings*, J. Lightwave Technol. **19**, 1352–1365 (2001).

[129] P. Arora, I.V. Il'ichev, A.V. Chamray, A.S. Kozlov, V.M. Petrov, J. Petter and T. Tschudi, *Integrated optical filter with fast electrically reconfigurable transfer function*, Proc. OFC, Paper JWA 23 (2007).

[130] P. Arora, A.S. Kozlov, I.V. Il'ichev, A.V. Chamray, V.M. Petrov, J. Petter and T. Tschudi, *Synthesis of the transfer function of a spectral bragg filter using electro-optical phase-shift keying*, Proc. CLEO, Paper CMG 5 (2007).

[131] C. Heinisch, S. Lichtenberg, V.M. Petrov, J. Petter and T. Tschudi, *Phase-shift keying of an optical bragg cell filter*, Opt. Comm. **253**, 320–331 (2005).

[132] C. Heinisch. *Synthese der Transferfunktion abstimmbarer optischer Filter durch Phase-Shift-Keying von Bragg Gittern.* Master's thesis, Institut für Angewandte Physik, TU Darmstadt, 2005.

[133] S. Lichtenberg. *Manipulation of holographic gratings using phase shift keying.* Dissertation, Institut für Angewandte Physik, TU Darmstadt, 2007.

[134] C. Heinisch, S. Lichtenberg, V.M. Petrov, J. Petter and T. Tschudi, *Dynamic bragg filter with a synthesized spectral transfer function*, OSA Trends in Optics and Photonics (TOPS) **99**, 738–743 (2005).

[135] R.C. Alferness, C.H. Joyner, M.D. Divino, M.J.R. Martyak and L.L. Buhl, *Narrowband grating resonator filters in InGaAsP/InP waveguides*, Appl. Phys. Lett. **49**, 125–127 (1986).

[136] K. Utaka, S. Akiba, K. Sakai and Y.Matsushima, $\lambda/4$*-shifted InGaAsP/InP DFB lasers*, IEEE J. Quantum Elec. **22**, 1042–1051 (1986).

[137] J. Canning and M.G. Sceats, π*-phase-shifted periodic distributed structures in optical fibers by UV-post processing*, Elec. Lett. **30**, 1344–1345 (1994).

[138] R. Kashyap, P.F. Mckee and D. Armes, *UV written reflection grating structures in photosensitive optical fibers using phase-shifted phase-masks*, Elec. Lett. **30**, 1977–1978 (1944).

[139] M. Janos and J. Canning, *Permanent and transient resonances thermally induced in optical fiber bragg gratings*, Elec. Lett. **31**, 1007–1009 (1995).

[140] M.A. Rodriguez, M.S. Malcuit and J.J. Butler, *Transmission properties of refractive index-shifted bragg gratings*, Opt. Comm. **177**, 251–257 (2000).

[141] N.Q. Ngo, S.Y. Li, L.N. Binh and S.C. Tjin, *A phase-shifted linearly chirped fiber bragg grating with tunable bandwidth*, Optc. Comm. **260**, 438–441 (2006).

[142] C.J.S. de Matos, P. Torres, L.C.G. Valente, W. Marguilis and R. Stube, *Fiber bragg grating characterization and shaping by local presuure*, J. Lightwave Tech. **15**, 1206–1211 (2001).

[143] T. Erdogan, *Fiber grating spectra*, J. Lightwave Tech. **15**, 1277–1294 (1997).

[144] W.C. Wang, M. Fischer, A. Yacoubian and J. Menders, *Phase-shifted bragg grating filters in polymer wavegudies*, IEEE Photon. Tech. Lett. **15**, 548–550 (2003).

[145] L. Zhu, Y. Huang, W.M.J. Green and A. Yariv, *Polymeric multi-channel bandpass filters in phase-shifted bragg waveguide gratings by direct electron beam writing*, Opt. Exp. **12**, 6372–6376 (2004).

[146] V.M. Petrov, S. Lichtenberg, J. Petter and T. Tschudi, *Control of the optical transfer function by phase-shift keying of a holographic bragg grating*, Opt. Comm. **229**, 131–139 (2004).

[147] S. Lichtenberg, C. Heinisch, V. Petrov, J. Petter and T. Tschudi, *Refractive-index measurement of gases with a phase-shift keyed interferometer*, Appl. opt. **44**, 4659–4665 (2005).

[148] M.A. Rodriguez, M.S. Malcuit and J.J. Butler, *Transmission properties of refractive index-shifted bragg gratings*, Opt. Comm. **177**, 251–257 (2000).

[149] J. Hong, W. Huang and T. Makino, *On the transfer matrix method for distributed-feedback waveguide devices*, J. Lightwave Tech. **10**, 1860–1868 (1992).

[150] B. Jacobsson, V. Pasiskevicius and F. Laurell, *Tunable single-longitudinal-mode ErYb:glass laser locked by a bulk glass bragg grating*, Opt. Lett. **31**, 1663–1665 (2006).

[151] B.L. Volodin, S.V. Dolgy, E.D. Melnik, E. Downs, J. Shaw and V.S. Ban, *Wavelength stabilization and spectrum narrowing of high-power multimode laser diodes and arrays by use of volume bragg gratings*, Opt. Lett. **29**, 1891–1893 (2004).

[152] Y. Park, S-T Lee and C-J Chae, *A novel wavelength stabilization scheme using a fiber grating for WDM transmission*, IEEE Phot. Tech. Lett. **10**, 1446–1448 (1998).

[153] J. Skaar, L. Wang and T. Erdogan, *On the synthesis of fiber bragg gratings by layer peeling*, IEEE J. Quantum Elec. **37**, 165–173 (2001).

[154] L. Poladian, *Simple grating synthesis algorithm*, Opt. Lett. **25**, 787–789 (2000).

Acknowledgements

Since the time I started as a fresher in the research field till the completion of this doctoral thesis, my journey in the last three years has been arduous, wavering at times and yet very fulfilling. Apart from almighty God, there are many people to whom I owe tremendous thanks for helping and supporting me to make this journey reach its destination.

I express my deep sense of gratitude and indebtedness to Prof. Dr. Theo Tschudi for providing me with opportunity to be a part of his research group and for giving me the possibility to prepare and finish dissertation. His open and supportive supervision allowed me to work with innovative ideas in a healthy working environment. I want to thank him for his enthusiastic guidance, constructive comments and suggestions for the successful completion of this work. I am grateful to him for granting me the possibility to present my work at several national and international conferences.

My sincere thanks and special appreciation to the group leader of the photorefractive optics group, Dr. Jürgen Petter for his invaluable help and scientific as well as moral support. Being leader of the group, he managed a friendly and comfortable working environment for me. His motivational words and positive attitude always encouraged me to perform better. He is the one, whom I could always rely on for all kinds of personal or professional problems. I am personally indebted to him for endless corrections of scientific texts and also for boosting up my morale everytime I felt dejected.

I express deep gratitude to Dr. V. M. Petrov for his invaluable advises and encouragement throughout the work. His guidance for my work and detailed discussions with him have aided to make this work fruitful. He has been a constant source of encouragement and has always helped me to improve the quality of my work.

Words are inadequate to express thanks to Mr. Gerhard Jourdan, who patiently examined numerous samples with SEM technique. His expertise and experience helped me in better examination of the samples. His technical assistance helped me complete this work in time. I offer my most sincere thanks to him for helping me always with a nice smile.

I express special thanks to my colleagues Dr. Sören Lichtenberg and Dr. Ralf Nicolaus for their constant help, suggestions and encouragement throughout my work. I am very much grateful to my colleagues Christian Heinisch and Jörn Peuser for constructive scientific and technical discussions.

Furthermore, I would like to acknowledge scientific and moral support from all the members of the group. I would especially like to thank Julia Hahn, Markus Tiemann and Sebastian Schiffner for the pleasurable working environment and for always being there for any kind of help. I am also very thankful to our dear secretary Ms. Ellen Happel for taking care of the administrative tasks and for lending help in all sorts of problems.

I am also thankful to all the members of the Institute of Applied Physics, who helped me in any little way. I would also like to acknowledge support from mechanical and electrical workshop for preparing various mounts and circuits needed for the experiments.

I would like to gratefully acknowledge DFG (German Research Foundation) for the financial support and also for providing the opportunity to work in an interdisciplinary project. I would like to thank all members of the Graduiertenkolleg especially Prof. Dr. Peter Meissner, Benjamin Kögel, Sanghyun Seo, Robert Schafranek and Sandro Jatta for their scientific and technical support.

I would like to take a moment to thank my husband Debasish Banerjee who is a source of continuous inspiration and encouragement for me. Without his love and support, I would not have been able to complete and compile this work. He is the one who supported me at all times whether it was frustration or success. He made me smile even in dejection, made me work harder even after failure and took care of my food and health when I was totally indulged in work. I cannot thank him enough for everything.

Most important of all, I am grateful to my parents, my in-laws and my entire family for their constant love, endless support and for making me the person I am today. Without their prayers and blessings this work surely would not have been possible. Last but not the least, I would specially like to thank my brother Sanjay Arora for having immense faith in me and for always encouraging me to achieve higher goals in life.

Darmstadt, in October 2007.

Zusammenfassung (Conclusion in German)

Aufgrund ihrer charakteristisch schmalbandigen Filtereigenschaft sind Bragg-Gitter in optischen Nachrichtennetzen weit verbreitet. Durch die schnell voranschreitende Entwicklung in diesem Bereich müssen auch auf Bragg-Gittern basierende Filter und Schaltelemente zu abstimmbaren und rekonfigurierbaren Elementen weiterentwickelt werden. Gegenstand dieser Arbeit ist die Untersuchung, Konzeption und Kontrolle elektro-optisch abstimmbarer Bragg- Gitter für die Anwendungen in der optischen Telekommunikationstechnik. Hier wird besonders das "elektro-optische Phase Shift Keying" vorgestellt, durch das ein gezieltes Design (Synthese) gewünschter Filterfunktionen ermöglicht wird. Die Untersuchung der Bragg-Gitter erfolgt hierbei durch das spektrale Auslesen der am Gitter reflektierten Intensität, die in dieser Arbeit als Transferfunktion ("transfer function") bezeichnet wird und die Informationen über das Phasen- und Amplitudenprofil des zu Grunde liegenden Gitters enthält.

Zur Untersuchung der elektro-optischen Eigenschaften wurden zu Beginn dieser Arbeit schnell schaltbare Linsen und Spiegel als photorefraktive Volumengitter in Lithium Niobat Volumenkristallen realisiert und untersucht. Aufbauend auf diesen Ergebnissen wurden photorefraktive Gitter in Wellenleiterstrukturen in $LiNbO_3$-Kristallen eingeschrieben und erfolgreich die elektro-optische Abstimmung der Filterfunktion integriert optischer Filter demonstriert. Bei diesen Untersuchungen wurden, meines Wissens zum ersten Mal, die nichtlinearen spektralen Reflexionseigenschaften photorefraktiver Bragg-Gitter als Wellenlängenfilter diskutiert. Im Hauptteil der Arbeit wird das Konzept des "elektro-optischen Phase Shift Keyings" (e-o PSK) vorgestellt und dessen Potential zur schnellen und dynamischen Abstimmung der Filter-Transferfunktion untersucht. Zum ersten Mal wird hier die segmentweise elektro-optische Abstimmung eines zuvor eingeschriebenen homogenen Bragg-Gitters zur schnellen ($< 1\mu$s) dynamischen Neukonfiguration bzw. zur Synthese einer Filterfunktion angewendet.

Die Arbeit beginnt mit der Diskussion des theoretischen Hintergrundes zur Beugungsanalyse an Volumen-Bragg-Gittern. Hierbei wurde im Besonderen auf die für meinen Fall wichtigen Reflexionseigenschaften der Gitter und auf die zugehörigen Parameter (Gitterlänge, Gitterperiode, Kopplungsstärke und Abweichung von der Bragg-Bedingung) eingegangen. In diesem Zusammenhang wurde hier auch Kogelniks "coupled wave theory" diskutiert.

In Kapitel 3 schließt sich eine Darstellung der prinzipiellen Eigenschaften des photorefraktiven Effektes und der zu Grunde liegenden Ladungstransportmechanismen an. Im Speziellen wurden in diesem Abschnitt die photovoltaischen und elektro-optischen Eigenschaften des von mir in meinen Experimenten verwendeten $LiNbO_3$ untersucht.

Zur Untersuchung der elektro-optisch kontrollierten Beugung an photorefraktiven Volu-

mengittern wurde zunächst das Verfahren des "Electric-Field-Multiplexing" (EFM) an schnell schaltbaren holographischen Linsen und Spiegeln in $LiNbO_3$-Volumenkristallen realisiert. In ausführlichen Berechnungen wurden hierfür die optimalen Parameter (Kristalldimensionierung und -geometrie, Aufzeichnungs- und Elektrodenanordnung, angelegte Spannung) ermittelt. Zur Verringerung der "Electric Field Selectivity" (EFS) sollte in der von mir verwendeten Reflektionsgeometrie bei möglichst kleiner Gitterperiode die Länge des Gitters möglichst groß sein. In Anbetracht der Anforderungen an die anzulegende Spannung wurde die optimale Kristallgeometrie bestimmt; hier konnte für den Fall außerordentlicher Polarisation der Winkel zwischen dem extern angelegten Feld und der C-Achse des Kristalls zu 40°-50° bestimmt werden. Nach der Vermessung von vier Kristallproben wurde der Wert der EFS zu ± 2kV/cm bestimmt. Durch Aufnahme der Hologramme von zwei Objektiven mit 40 cm bzw. 60 cm Brennweite konnte ich zwei schnell elektro-optisch schaltbare holographische Linsen entsprechender Brennweite herstellen. Die volumenholographische Aufnahme von zwei unterschiedlich positionierten Spiegeln ermöglichte mir die Demonstration von schnell elektro-optisch schaltbaren Strahldeflektoren, die auf einer Kombination von Winkel- und Elektrischem Feld-Mutliplexing beruhen. In meinen Experimenten konnte ich einer Strahlablenkung von 50,32° erreichen. Die Analyse der Zeit für den Umschaltvorgang ergab eine Schaltzeit von 100 μs, die unabhängig vom Winkel der Strahlablenkung und in diesem Fall nur durch die Kristallgeometrie begrenzt ist, da der Kristall für das System einen kapazitiven Widerstand darstellt.

Auf diesen Untersuchungen basierend diskutiere ich in Kapitel 5 die elektro-optische Kontrolle der Beugung an Bragg-Gittern in Wellenleiterstrukturen. Nach einer kurzen Einführung in die Theorie der Wellenleiter und der Wellenkopplung bei der Beugung an Gitterstrukturen wird hier die Herstellung der von mir verwendeten photorefraktiven und photolithographischen Gitter präsentiert. Um die Bragg-Filter in Reflektion auf Telekommunikationswellenlängen (1550 nm) abzustimmen wurden in den durch Titaneindiffusion in $LiNbO_3$ eingebrachten Wellenleiter in Transmissionsgeometrie Volumengitter mit einer Periode von ca. 350 nm aufgezeichnet. Mit photorefraktiv eingeschriebenen Gittern konnten Beugungseffizienzen von mehr als 90% bei einer Bandbreite von 0,16 nm bei der mittleren Wellenlänge von 1555 nm erzeugt werden. Während meiner Untersuchung der Beugung bei Reflexion an einem photorefraktiven Volumengitter konnten ich hierbei zum ersten Mal nichtlineare Reflexionen höherer harmonischer Komponenten der reflektieren Wellenlänge nachgewiesen. Der Effekt der spektralen Verschiebung der Reflexionen höherer harmonischer Komponenten ist ein wichtiger Gesichtspunkt bei der Herstellung effektiver Filterelemente.

Im Gegensatz zu den photorefraktiven Gittern bieten photolithographisch eingeschriebene gerippte (oder "corrugated") Gitter eine dauerhafte Haltbarkeit und die Möglichkeit der Massenproduktion. Im zweiten Teil des 5. Kapitels wird ausführlich die von mir angewendete Herstellungsmethode der gerippten Gitter dargestellt. Zunächst wurde in den auf dem Wellenleiter aufgebrachten Photoresist ein holographisches Gitter aufgezeichnet. Das darauf in Schattenverdampfungstechnik aufgebrachte Chrom dient bei dem darauf folgenden reaktiven Ionen-Ätzen (RIE) als harte Maske, um die Gitterstruktur effektiv in den Wellenleiter zu übertragen. Nach dem Anbringen von "pigtailed" Fasern an die Enden des

Wellenleiters und dem Aufbringen eines Schutzüberzuges konnte die Transferfunktion des Filters vermessen die Bandbreite wurde hierbei zu 0,17 nm bei einer mittleren Wellenlänge von 1555 nm bestimmt. Durch das Anlegen eines elektrischen Feldes von $\pm$ 10 V/μm an die Elektroden auf beiden Seiten des Wellenleiters konnte daraufhin die mittlere Wellenlänge der Transferfunktion um 0,3 nm kontinuierlich abgestimmt werden.

In den weiterführenden Untersuchungen wurde, wie in Kapitel 6 ausgeführt, der Einsatz der elektro-optischen Abstimmung integrierter Bragg-Gitter durch das Verfahren des "elektro-optischen Phase-Shift Keyings" erweitert. In diesem Fall wird der globale Brechungsindex des Wellenleitermaterials nicht durch ein homogenes externes elektrisches Feld verändert, sondern durch eine gezielte Strukturierung des Feldes räumlich moduliert. Diese Feldmodulation wurde erreicht, indem neben dem Wellenleiter 8 gleich große Paare von Elektroden aufgebracht wurden, an die jeweils eine individuelle Spannung angelegt werden konnte. Die sich daraus ergebene räumliche Brechungsindexmodulation des Materials, in dem der Wellenleiter eingeschrieben ist, erzeugte in dem über dem Wellenleiter homogenen Gitter eine räumlich modulierte Phasenverschiebung, durch die sich die Transferfunktion gezielt spektral verändern lässt.

Nach der Darstellung der Grundprinzipien des Phase-Shift-Keyings und der Erweiterung des zu Grunde liegenden theoretischen Modells der Theorie gekoppelter Wellen auf strukturierte Bragg-Gitter, stelle ich die experimentelle Realisierung mehrerer, durch e-o PSK gezielt modulierter Transferfunktionen vor. So konnte ich, nach meinem Kenntnisstand zum ersten Mal, das schnelle dynamische Abstimmen einer (Filter-) Transferfunktion, das Umschalten einer Pass-Band in eine Stopp-Band Filterfunktion, die Synthese von Zwei-, Drei- und Fünf-Band Filterfunktionen, sowie das Konfigurieren einer "Flat-Top" Filterfunktion demonstrieren. Über dies hinaus konnte ich in meinen Experimenten zeigen, dass durch das Verfahren des e-o PSK eine schnelle Korrektur der Form und der Lage von Filtertransferfunktionen möglich ist. Die experimentellen Ergebnisse stimmen hierbei hervorragend mit den theoretischen Berechnungen überein. Ein weiterer großer Vorteil der Abstimmung und Synthese von Transferfunktionen durch das e-o PSK ist gegenüber bisher etablierten Verfahren neben der hohen Flexibilität im Design der Filterfunktion vor allem die hohe Schaltgeschwindigkeit. So konnte ich in meinen Untersuchungen die Schaltzeit zwischen zwei beliebigen Filterfunktionen auf weniger als 1μs bestimmen.

Die von mir untersuchte Möglichkeit des elektro-optischen Phase-Shift Keying erlaubt somit die Herstellung schnell rekonfigurierbarer und flexibler integriert-optischer Filter für die Anwendung in bestehenden optischen DWDM-Nachrichtennetzen sowie auch für zukünftige rekonfigurierbare OCDMA (Optical Code Divisin Multiple Access)-Netze.

Curriculum Vitae

Personal Data

Name:	Poonam Arora
Date of birth:	28. July 1980
Place of birth:	Rohtak Haryana, India
Marital status:	married

School Education

1983-1995	Basic schooling in Hisar
1995-1997	Senior Secondary Examination at D.N.P.G College in Hisar

Higher Studies

7/1997-6/2000	Bachelor of Science (B.Sc.) from Kurukshetra University Kurukshetra
7/2000-6/2002	Master of Science (M.Sc) in Physics from Indian Institute of Technology (IIT) Delhi
7/2002-6/2004	Master of Technology (M.Tech) in Applied Optics from Indian Institute of Technology (IIT) Delhi
9/2003-5/2004	Master thesis with DAAD scholarship under supervision of Prof. Dr. T. Tschudi and Prof. K. Singh at Institute of Applied Physics, Technische Universität Darmstadt Title: *Electrically controlled light diffraction from volume photorefractive gratings*

Graduation (Ph.D. thesis)

since 9/2004	Ph.D. student under the supervision of Prof. Dr. T. Tschudi at Institute of Applied Physics, Technische Universität Darmstadt

Eidesstattliche Erklärung

Hiermit erkläre ich an Eides Statt, die vorgelegte Dissertation selbständig, nur mit den angegebenen Hilfsmitteln angefertigt, und bisher keinen Promotionsversuch unternommen zu haben.

Darmstadt, den 16. Oktober 2007

(Poonam Arora)